

Current issues and problems in laser welding of automotive aluminium alloys

H. Zhao, D. R. White, and T. DebRoy

The automotive industry is facing demands simultaneously to increase its fleet average fuel economy and to reduce the emission of greenhouse gases by its products. In order to meet these new standards, the industry is increasingly aiming to decrease the weight of vehicles through the use of new materials, especially lightweight aluminium alloys. Laser welding is a critical enabling technology in reducing the weight of the body structure through increased use of aluminium and tailor welded blanks. In this review the available research on the laser welding of 5xxx, 6xxx, and some 2xxx series automotive aluminium alloys is critically examined and interpreted from different perspectives. First, the current understanding of the important physical processes occurring during laser welding of these alloys such as energy absorption, fluid flow and heat transfer in the weld pool, and alloying element vaporisation are examined. Second, the structure and properties of these weldments are critically evaluated. Third, commonly encountered defects found in laser welded automotive grade aluminium alloys and their science based remedies are discussed. Finally, several important unanswered questions related to laser welding are identified and an outlook on future trends in the laser welding of automotive grade aluminium alloys is presented. The review is written for scientists and materials engineers who are not specialists in welding, practising engineers in the automotive industry, welding engineers, and researchers in this field.

IMR/345

© 1999 IoM Communications Ltd and ASM International. Mr Zhao and Professor DebRoy are in the Department of Materials Science and Engineering, The Pennsylvania State University, University Park, PA 16802, USA and Dr White is at Ford Research Laboratory, Ford Motor Co., Dearborn, MI, USA.

Introduction

As environmental awareness grows among consumers as well as government agencies, attempts to improve fuel economy in automobiles are accelerating. In addition to improved powertrain efficiency, vehicle weight reduction is an important factor. The ability of a steel body structure to deliver weight savings is limited, so use of aluminium in autobody structures is increasing, and is projected to expand further in the next decade.

Body architecture is also likely to undergo change in the near future. Tailor welded blanks are becoming increasingly common; most commonly implemented in steel today, the need for tailor welded blanks in aluminium is growing. Tailor welded blanks offer reduced weight with increased design flexibility, and can reduce material usage. Since safety is also a

growing public concern, some vehicle architecture changes may be needed to offset issues surrounding the relationship between vehicle weight and safety, with increasing use of spaceframes, or spaceframe subassemblies expected. Increased use of technologies such as hydroforming that can be used to produce complex single piece sections, further decreasing weight, while enhancing structural strength and stiffness, will also be seen. All of these technologies are likely to be implemented in aluminium as well as in steel, as the weight of the body structure drops.

Inevitably, this will lead to needs for new joining technologies for automotive aluminium alloys. Resistance spot welding (RSW) is the most important welding process now used in autobody construction. While RSW is a nearly ideal process for the assembly of stamped steel body structures, offering robustness and low cost, it is more costly and less robust when used on aluminium structures. Further, increased use of closed sections made via hydroforming will require processes other than RSW. Introducing tailor welded blanks in aluminium will also require new joining capability to support high volume production.

Laser welding is a particularly interesting approach to the construction of advanced automotive body structures because of its high speed, low heat input, and flexibility. Among laser welding's potential benefits are thinner flanges, the ability to produce tailor welded blanks, and reduced distortion in hydroformed frame structures. New developments in laser technology, such as fibre optic delivery of YAG laser energy, have enhanced its ability to be used in high volume automation, while solid state laser diodes promise lower prices in the near future. Since future vehicle structures are likely to be composed of a much wider variety of materials than today, including mild steel, high strength steel, and aluminium, a single power source will reduce capital investment, and increase flexibility in an age of increasing 'mass customisation'.

Application of laser welding to aluminium, and in particular the 5xxx and 6xxx alloys which will constitute the bulk of automotive production, is far from a mature technology. Fundamental questions remain open, ranging from laser coupling with aluminium to the chemistry and physical metallurgy of the resulting joints. Current issues and problems in the laser welding of automotive aluminium alloys will be reviewed. First, the current understanding of the important physical processes occurring during laser welding of these alloys, including energy absorption, fluid flow and heat transfer in the weld pool, and vaporisation of alloying elements at the weld pool surface will be examined. Second, the microstructural features and mechanical properties of the weldment will be critically evaluated. Third, the commonly encountered defects, including porosity and hot cracking, found in

laser welding automotive grade aluminium alloys and their science based remedies will be analysed, considering both the physical processes in the welding and the structure of these alloys. Finally, several important unanswered questions related to this welding will be identified and an outlook on future trends in the laser welding of automotive grade aluminium alloys will be presented.

Energy absorption

Energy transfer efficiency

Energy transfer efficiency is defined as the ratio of the energy absorbed by the irradiated materials to the laser output energy. During conduction mode laser welding, the energy transfer efficiency is equivalent to the absorptivity of the metal. On the other hand, when a keyhole is formed during laser welding, the energy transfer efficiency can be much larger than the absorptivity of the metal because of multiple reflections within the keyhole.

The absorption of laser energy by metals depends largely on conductive absorption by free electrons. For clean metal surfaces the absorptivity can be calculated from the electrical resistivity of the metal substrate. Hagen and Rubens¹ first developed approximate formulas for calculating the emissivity of polished metals from experimental study. Combined with Kirchhoff's law that the emissivity is equal to the absorptivity at the same temperature and wavelength for internally non-reflecting media, their findings led to the following relation for absorptivity in the normal direction

$$\eta_{\lambda}(T) = \varepsilon_{\lambda}(T) = 0.365(r/\lambda)^{1/2} \quad \dots \quad (1)$$

where $\eta_{\lambda}(T)$ and $\varepsilon_{\lambda}(T)$ are the absorptivity and emissivity at temperature T and wavelength λ , r is the resistivity (Ω cm) at temperature T , and λ is the wavelength (cm). Bramson² developed a more accurate formula for absorptivity using the series expansion:

$$\eta_{\lambda}(T) = \varepsilon_{\lambda}(T) = 0.365(r/\lambda)^{1/2} - 0.0667(r/\lambda) + 0.006(r/\lambda)^{3/2} \quad \dots \quad (2)$$

Calculations using equation (2) are accurate during vertical laser irradiation of clean metal surfaces in vacuum when a plasma plume is not formed. Equation (2) indicates that the absorption of laser energy is determined by the wavelength of the laser and the resistivity of the metal. However, several other factors such as the nature of the surface, the joint geometry, the size and nature of the plasma existing above the weld pool, and the concentration of volatile alloying elements in the metal also affect the absorption of laser energy during welding. The absorption of laser energy by materials becomes more efficient as the laser wavelength decreases. The solid state Nd-YAG laser with a characteristic wavelength of 1.06 μ m provides better coupling with aluminium than the CO₂ laser with a characteristic wavelength³ of 10.6 μ m.

Experiments^{4,5} show that the absorption of laser beam energy by aluminium is very low. The poor coupling of the laser energy is due in part to the high density of free electrons in the solid, which makes

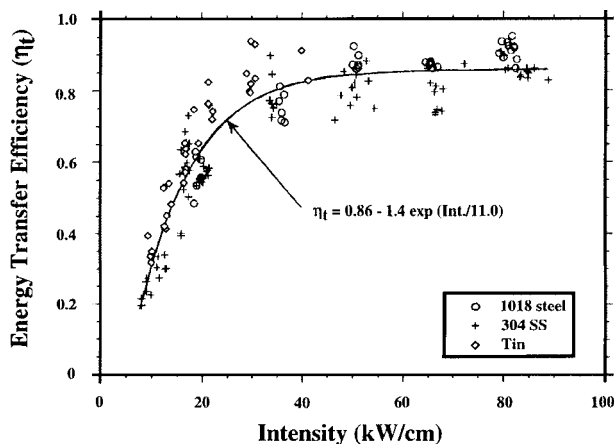
aluminium one of the best reflectors of light. Huntington and Eagar⁴ studied the absorption of CO₂ laser beam energy by pure aluminium and 5456 aluminium alloy by calorimetry. Table 1 summarises the extent of absorption of a 200 J, 2 s pulse laser beam following different surface preparations. It is noted that the energy absorption is low on the as received samples and considerable scatter in the measured absorption exists due to local differences in oxide thickness and surface roughness. Compared with as received samples, sandblasting and anodising significantly increase, whereas electropolishing somewhat decreases, the absorption of the laser beam energy. It was believed that the increased absorption of the anodised specimen was due to the decreased free electron concentration at the surface, whereas in the case of sandblasting, the increased absorption was thought to be due to light absorption by glass beads embedded in the surface.⁴ The reduced absorption of the electropolished specimen appeared to be due to the high reflectivity of the smooth surface. It is also observed from the data in Table 1 that 5456 alloy has an absorption coefficient about 20–25% higher than that of pure aluminium with the same surface preparation, which can be explained by lower free electron concentration in the 5456 alloy.⁴ Marsico⁵ measured the absorption of a CO₂ laser beam by 5083 and 7039 aluminium alloys. The absorption of a 220 J, 2 s pulse was found to be in the range 12–15% by 5083 alloy and 6.9–9.0% by 7039 alloy. The difference in absorption was attributed to the difference in composition of the two alloys. All the above results were obtained when a flat surface was irradiated by a laser beam without any keyhole formation. Under such conditions, the absorption of laser beam energy by aluminium and its alloys is very low.

The formation of a keyhole greatly increases the absorption. The minimum power density required for keyhole formation is about 10⁶ W cm⁻² for the CO₂ laser welding of aluminium alloys.³ This threshold power density is considerably lower for Nd-YAG laser welding of the same materials.³ The enhanced absorption is believed to be contributed by the multiple reflections of the laser beam in the cavity.⁶ Huntington and Eagar⁴ studied the effects of keyhole formation and joint geometry on laser beam absorption by pure aluminium and 5456 alloy. They found that the absorption increased drastically at a certain value of laser beam power and showed that the dramatic increase in absorption was due to the formation of a keyhole rather than the onset of melting as commonly believed.^{7,8}

Experiments^{9–11} on laser welding of aluminium alloys show that there exists a threshold laser power density above which a keyhole is formed and coupling of the laser beam with the welded materials drastically

Table 1 Power absorption from 200 J, 2 s laser pulse,⁴ %

Surface preparation	5456 Al alloy	99.999%Al
Anodised	27	22
Sandblasted	22	20
As received	5–12	7
Electropolished	4	5



1 Effect of laser beam intensity on measured heat transfer efficiency for CO₂ laser welding of 1018 steel, 304 stainless steel, and tin¹³

increases. Since a keyhole is formed primarily by the recoil force of the vaporising atoms, high concentration of volatile elements in weld metal is helpful in the formation of a keyhole. Katayama¹² reviewed the melting of aluminium alloys by laser beam and rated ease of melting, from easy to difficult, as follows: 2090 < (5456, 5083, and 5182) < (7075 and 7N01) < 5052 < (2024, 6061, and 6N01) < (2219 and 3003) < (1100 and 1050). These results indicate that alloys with higher concentration of volatile elements such as lithium in 2090, magnesium in 5xxx alloys, and zinc in 7xxx alloys, are more easily melted by the laser beam. The volatile alloying elements, owing to their high vapour pressures, aid in the establishment of the keyhole and reduce the threshold power density required to achieve satisfactory coupling between laser beam and aluminium alloys.

Fuerschbach¹³ measured the energy absorption during CO₂ laser welding of 1018 steel, 304 stainless steel, and tin. Most of the measurements were carried out using power densities well above that required for keyhole formation. It was observed that the energy transfer efficiency was less dependent on the laser irradiance, defined as the laser power divided by the beam spot area at the focal point, than on the laser intensity, defined as the laser power divided by the diameter of the beam spot at the focal point. Therefore, the energy transfer efficiency was plotted¹³ as a function of the laser intensity as shown in Fig. 1. Despite the great differences in composition and physical properties, the measured values of energy transfer efficiency were found to be independent of material. The absorptivity increased from 0.20 to 0.90 with increase in laser beam intensity and stabilised at approximately 0.90 at intensities greater than 30 kW cm⁻¹ (Fig. 1). The results indicate that the absorption of laser energy is similar for different materials in the keyhole mode welding regime. An empirical relationship between the energy transfer efficiency and laser power intensity was obtained for the three materials as shown in Fig. 1. However, the applicability of this formula to the CO₂ laser welding of aluminium alloys has not been examined.

Independent of the mode of welding, pronounced vaporisation of the volatile alloying elements may

result in the formation of a plasma plume that can absorb¹⁴ and scatter¹⁵ a part of the laser beam energy. The plasma reradiates^{16,17} the laser energy in all directions as shorter wavelength photons which are more readily absorbed by the material than the original laser light. When the plasma is small in size and is confined near the weld pool surface, it may aid in the coupling of the laser beam with the workpiece due to efficient absorption of the reradiated energy by the workpiece. However, when the plasma plume grows in size, it absorbs a significant amount of laser energy,^{18,19} resulting in less absorption by the workpiece.

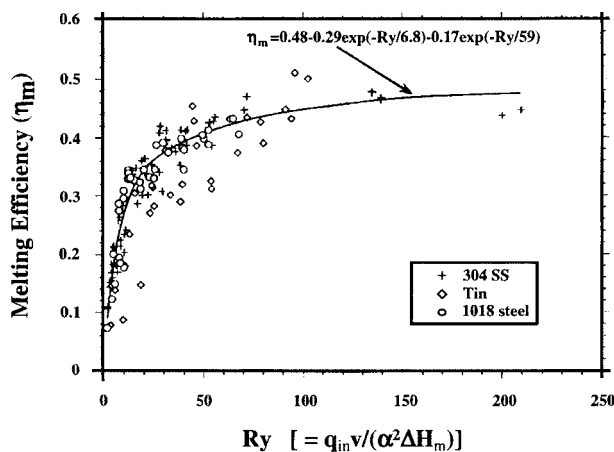
Huntington and Eagar⁴ showed that optimising joint geometry can improve the absorption of laser energy. To study the effect of joint geometry on absorption, welds were made on bead on plate, V groove, and square groove with the same laser beam power. The fusion zone cross-section areas on V groove and square groove were much greater than that of bead on plate welds, indicating better absorption of laser beam energy in grooved joints. The square groove joints were found to be very sensitive to geometric changes, which could significantly alter the beam absorption. On the other hand, V groove joints were found to be desirable for both weld consistency and efficient use of laser beam energy.

Melting efficiency

Melting efficiency, which is defined as the ratio of heat necessary just to melt the base metal to the heat absorbed by the workpiece, is another important parameter in evaluating energy absorption in welding processes. Fuerschbach¹³ found that the melting efficiency η_m in CO₂ laser welding of 1018 steel, 304 stainless steel, and tin could be correlated with a modified Rykalin number Ry

$$\eta_m = 0.48 - 0.29 \exp(-Ry/6.8) - 0.17 \exp(-Ry/59) \quad (3)$$

$Ry = q_{in} v / (\alpha^2 \Delta H_m)$, where q_{in} is the net power absorbed by the workpiece, v is welding speed, α is the thermal diffusivity of the workpiece at the liquidus temperature, and ΔH_m is the enthalpy of melting. Figure 2 shows that although there is considerable scatter in the data, the proposed correlation provides a useful framework for understanding melting efficiency of different alloys. Equation (3) indicates that the melting efficiency is determined by the welding parameters q_{in} and v , and the thermal properties of the workpiece α and ΔH_m . Aluminium has much higher thermal diffusivity than other common metals. Therefore, under the same welding conditions, the dimensionless number Ry is much lower for aluminium than for other alloys, resulting in a lower melting efficiency. In order to obtain satisfactory melting efficiency, high values of q_{in} and v are required. Since the value of q_{in} is determined by the laser output power and the absorptivity of the laser energy by the workpiece, operating at the maximum laser output power and maintaining the keyhole mode of welding are desirable to achieve high melting efficiency. On the other hand, increasing welding speed also increases melting efficiency. However, Fuerschbach¹³



2 Dependence of laser melting efficiency on dimensionless parameter Ry for CO_2 laser welding of 1018 steel, 304 stainless steel, and tin¹³

also found that extremely high welding speeds may decrease melting efficiency if the welding mode is shifted from keyhole mode to conduction mode. Therefore, the use of high laser power and high welding speed while maintaining keyhole mode welding is helpful in obtaining good melting efficiency in continuous fusion welding.

Heat transfer and fluid flow

Background

The variation of temperature with time, often referred to as the thermal cycle, affects the microstructure, residual stress, and distortion produced in a welded structure. At the weld pool surface, the temperature distribution affects the vaporisation of volatile alloying elements such as magnesium and zinc, the absorption and desorption of hydrogen and other gases, and thus, the weldment composition. In the interior of the weld pool, depending on the local temperature, as well as composition, inclusions grow or dissolve. Thus, control of temperature profiles and cooling rates is important to ensure sound welds with desired fusion zone geometry, chemical composition, microstructure, and low residual stress. Therefore, understanding of heat and fluid flow in the weld pool is a prerequisite for understanding the geometry, composition, structure, and properties of the weld metal.

During laser welding, the interaction between the base metal and the heat source leads to rapid heating, melting, and vigorous circulation of the molten metal. For high power density beam welding such as laser welding, significant vaporisation of the weld metal may occur resulting in the formation of a keyhole within the molten pool. In the weld pool, the circulation of molten metal is driven by buoyancy, surface tension, and, when welding in the keyhole mode, by the vapour pressure. The resulting heat transfer and fluid flow affect the transient temperature distribution in the base material, the shape and size of the weld pool, and the solidification behaviour.

Knowledge of temperature profiles in the weld pool and in the adjacent solid region can provide insight

about heat during welding. However, the measurement of surface temperatures during fusion welding is difficult and requires specialised equipment, and no standardised procedure for measurement is currently available. Furthermore, a technique for the measurement of temperature within the molten weld pool still remains to be developed. Temperature measurement in the solid region commonly involves the placement of thermocouples in holes drilled in the plates. This practice is cumbersome and expensive, especially for thick plates. A recourse is to use quantitative calculations in order to understand heat transfer in fusion welding.

In the weld pool, heat is transported by convection and conduction. Because of its complexity, convective heat flow cannot be calculated analytically. As a result, most heat flow calculations in the past were limited to a simplified heat conduction calculation. Because of the availability of high speed computers in recent decades, more realistic and accurate heat transfer calculations considering both conduction and convection can now be performed. These complex calculations can predict temperature and velocity fields, weld pool geometry, and cooling rates. The computed values serve as a basis for understanding weld metal composition and, in simple systems, weldment structure. The verification of the computed values is often limited by measurement difficulties and, in many cases, the calculated results remain the only source of values.

Keyhole mode welding results in better energy coupling and higher penetration than conduction mode welding. Therefore, keyhole mode welding is usually preferred in industry. However, due to the complexity of the process, development of modelling of heat transfer, fluid flow, and mass transfer during keyhole mode welding is less vigorous than that of the available models of conduction mode laser welding. Therefore, much of the following discussion is pertinent to conduction mode welding, and modelling of transport processes in the keyhole mode welding is discussed separately.

Temperature and velocity fields

Measurements of temperature and liquid metal velocity in the weld pool have not been reported for the laser welding of automotive aluminium alloys. Furthermore, techniques for non-contact measurement of temperature during welding are still evolving. However, the fluid flow and heat transfer in all fusion welding processes share certain common features. Therefore, the findings from other fusion welding processes and results of welding of other alloys can provide useful information about the laser welding of aluminium alloys.

Schauer *et al.*²⁰ measured the temperature distributions in the keyhole during electron beam welding of several aluminium alloys, three steels, and tantalum, using a narrow band infrared radiation pyrometer. Their data showed that the peak temperature was the lowest for aluminium alloy welds and the highest for tantalum welds. They also observed that the presence of volatile elements such as magnesium and zinc in aluminium alloys significantly decreased

the weld pool peak temperature. As the contents of magnesium or zinc in aluminium alloys increase on moving from 1100 to 5083 to 7075 alloy, the average peak temperatures for these alloys decreased from a maximum of 2173 K for 1100 alloy to 1523 K for 5083 alloy and 1353 K for 7075 alloy. These results suggest that the higher the melting and boiling points of the weld metal, the higher the peak temperature in the weld pool. Heiple and Roper²¹ estimated the surface flow velocity of gas tungsten arc (GTA) weld pools by measuring the motion of particles using a high speed camera. They found that the velocities were in the range of 0.5 to 1.4 m s⁻¹, with an average value of 0.94 m s⁻¹. These velocities are fairly high considering the fact that a typical weld pool is only a few millimetres wide. Kraus²² obtained surface temperature profiles for GTA welding of some steels, using a non-contact laser reflectance measurement technique. The 'measurement' of pool temperature involved extrapolation of temperature versus time data after the arc is totally extinguished based on the perceived transient temperature profile before this time period. It is fair to say that reliable techniques for real time temperature measurement are still evolving.

Kou and Wang²³ calculated the fluid flow during CO₂ laser welding of 6061 aluminium alloy and obtained a maximum flow velocity of 3000 mm s⁻¹. Figure 3 shows the computed velocity and temperature fields in the laser melted pool of 6063 aluminium. The maximum computed temperature in the weld pool was found to be about 2273 K. The results show radially outward flow due to negative temperature coefficient of surface tension. The maximum velocity is of the order of 3 m s⁻¹ in a weld pool that is about 0.6 mm wide and 0.15 mm deep. The high computed velocities indicate that mixing in the weld pool is highly efficient. An important consequence of a well mixed pool is the absence of a significant spatial gradient of concentration of volatile components in the weld pool. Experimental data show that during laser welding of 5xxx series aluminium alloys the concentration of magnesium in the weld pool is fairly uniform,²⁴ although the concentration of this element is significantly lower than that in the base material. The large computed surface velocities are typical of surface tension driven flow in a weld pool. The fusion boundary computed from the temperature profiles agreed well with the experimentally determined wide and shallow weld pool profile.

It is known that the magnitude of the velocities for both buoyancy and electromagnetic force driven flows in the weld pool are usually much smaller than those obtained for surface tension driven flows.¹³ Kou and Wang²⁵ showed that during stationary GTA welding of 6061 aluminium alloy the maximum velocity caused by buoyancy, electromagnetic force, and surface tension force were 9, 180, and 3000 mm s⁻¹ respectively. The maximum velocity due to the combined effects of the three forces was 2300 mm s⁻¹. During laser welding, the surface tension force dominates due to the absence of electromagnetic forces.

The spatial gradient of surface tension is a stress, known as the Marangoni stress, which may arise owing to variations of both temperature and compos-

ition. Frequently, the convection in the weld pool results mainly from the stress that is determined by the temperature gradient at the weld pool surface. Assuming velocity distribution in a boundary layer, the maximum velocity u_m can be roughly estimated¹³ assuming that it occurs approximately halfway between the heat source axis and the weld pool edge

$$u_m^{3/2} = \frac{d\gamma}{dT} \frac{dT}{dy} (W^{1/2}/0.664\rho^{1/2}\mu^{1/2}) \quad \dots \quad (4)$$

where γ is the interfacial tension, T is the temperature, y is distance along the surface from the axis of the heat source, ρ and μ are the density and viscosity, respectively, and W is width of the weld pool. For a typical value of weld pool width of 5 mm, metal density of 2385 kg m⁻³, viscosity of 0.0013 kg m⁻¹ s⁻¹, temperature coefficient of surface tension $d\gamma/dT$ of -3.5×10^{-4} N m⁻¹ K⁻¹, and spatial gradient of temperature of 10⁵ K m⁻¹, the maximum velocity is approximately 1.65 m s⁻¹. The maximum velocity calculated from equation (4) can provide a rough idea of the maximum velocity of liquid metal in the weld pool. Detailed solutions of the equations of conservation of mass, momentum, and heat are necessary for the calculation of temperature and velocity fields in the weld pool.

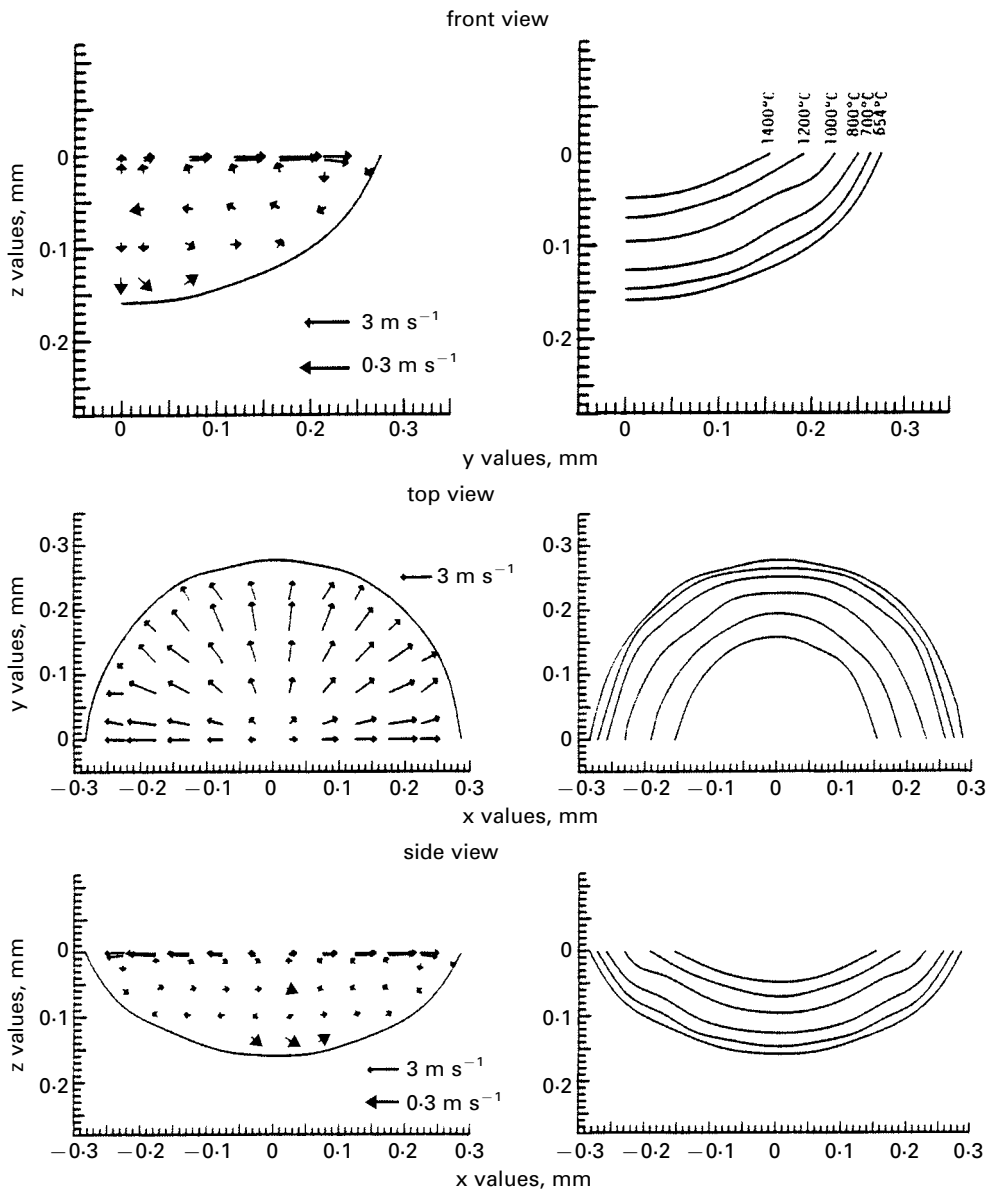
Both experiment²¹ and mathematical modelling²⁶ showed that the maximum velocities in steel weld pool were of the order of 1 m s⁻¹. On the other hand, the calculations of Kou and Wang^{23,25} obtained maximum velocities in the range of 2–3 m s⁻¹ for welding of 6061 aluminium alloy. These high velocities in aluminium alloy weld pools may lead to turbulence in the weld pool. Experimental determination of the velocities and temperatures in the weld pool remains a major challenge in the field.^{20–22} In the absence of adequate experimental work, contemporary literature relies heavily on the available recourse of numerical calculations of convective heat flow in the weld pool.

Relative importance of conduction and convection

The relative importance of conduction and convection in the overall transport of heat in the weld pool can be assessed from the value of the Peclet number

$$Pe = u\rho c_p L/k \quad \dots \quad (5)$$

where u is the velocity, ρ is the density, c_p is the specific heat at constant pressure, L is the characteristic length, and k is the thermal conductivity of the melt. For a typical case of welding aluminium with $\rho = 2385$ kg m⁻³, $c_p = 1080$ J kg⁻¹ K⁻¹, $L = 0.002$ m, and $k = 94.03$ W m⁻¹ K⁻¹, Pe is about $54.8u$. In the weld pool, the average velocity is considerably lower than the maximum velocity, very often by more than an order of magnitude. Thus, if the average velocity is of the order of 0.1 m s⁻¹, Pe is about 5.5. This value of Pe signifies that the transport of heat in the weld pool may be aided by both convection and conduction. The actual mechanism of heat transfer will depend on the value of the velocity, the size of the weld pool, and other parameters. Because of the high thermal conductivity of aluminium, if the velocity is low and the pool size is small, the value of Pe can



3 Calculated velocity and temperature fields in laser weld pool of 6063 aluminium alloy using CO₂ laser:²³ laser power 1.3 kW, welding speed 10 in min⁻¹

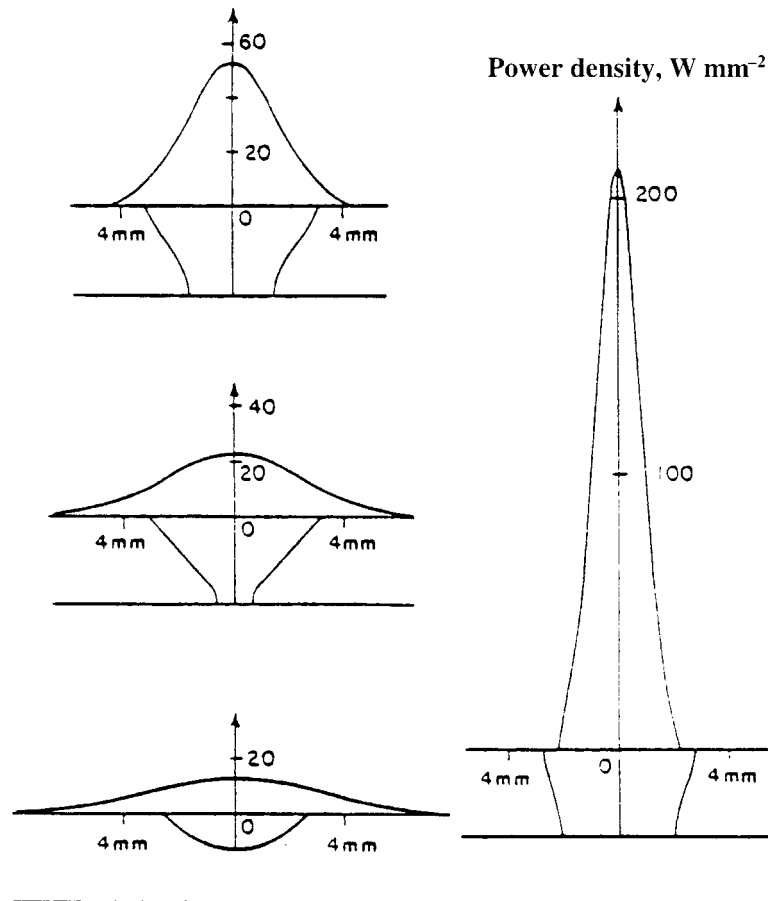
be low ($\ll 1$), and accurate calculations of heat transfer may be done under those conditions using relatively simple heat conduction calculations.

It is often instructive to compare the welding of aluminium with that of steels. For a typical case of the welding of steel, if we take $\rho = 7015 \text{ kg m}^{-3}$, $c_p = 795 \text{ J kg}^{-1} \text{ K}^{-1}$, $L = 0.002 \text{ m}$, and $k = 38 \text{ W m}^{-1} \text{ K}^{-1}$, Pe is about $294u$. Considering an average velocity of 0.1 m s^{-1} , the Pe obtained is about 29. When the Peclet number is $\gg 1$, the heat transport occurs primarily by convection, and heat conduction in the weld pool is not important. For the same size of the weld pool and same average velocity, the value of Pe for the welding of steels is much higher than that for the welding of aluminium. As a result, convective heat transport is much more important for the welding of steels than for the welding of aluminium alloys. It should also be noted that the conduction of heat in the solid region is very important for the dissipation of heat away from the weld pool. Therefore, the thermal conductivity of the solid and

the specimen dimensions are very important in determining the size of the molten pool.

Insight about heat transfer during welding of aluminium alloys can also be obtained by comparing properties of aluminium alloys with those of steels (Table 2). First, the thermal conductivity of aluminium alloys is nearly an order of magnitude higher than that of steels. Therefore, heat transfer by conduction is more efficient for aluminium alloys. When weld pool shape and size were calculated ignoring convection, the computed values matched well with the experimental results for stationary GTA welding of 1100 aluminium alloy while significant discrepancy between the two values was observed for AISI 304 stainless steel,²⁷ confirming that convective heat transfer is less important for aluminium alloys than for steels.

It is also useful to examine the Prandtl numbers of aluminium alloys and steels. The physical interpretation of the Prandtl number follows from its definition as a ratio of the kinematic viscosity ν to the thermal diffusivity α . The Prandtl number provides a measure



4 Four different power density profiles of heat source and their resultant welds:²⁸ laser power 860 W, welding speed 5.5 mm s⁻¹

of the relative effectiveness of heat transport by convection and diffusion in the velocity and thermal boundary layers, respectively. Near the fusion boundary of the molten weld pool where the fluid flow is stagnant, transport of heat by diffusion is more important than by convection. Since the Prandtl numbers of liquid aluminium and steel are much less than unity, the heat diffusion rate greatly exceeds the convection rate near the fusion boundary. Furthermore, since the Prandtl number of liquid aluminium is about one order of magnitude lower than that of iron, heat diffusion is more efficient in liquid aluminium alloys than in liquid steels.

Effect of power density distribution

Kou and Le²⁸ examined the effect of power density distribution on the weld pool shape for welding of 6061 aluminium alloy. In their model, an effective thermal conductivity was used to account for the effect of convection. The calculated results showed that the nature of the heat source greatly affected the weld pool shape and size. As shown in Fig. 4, for the same heat source power and welding speed, a focused heat source produced a deep and large weld pool. This is consistent with the result of a recent experimental study on Nd-YAG laser welding of 5182 and 5754 aluminium alloys.²⁴ As shown in Fig. 5, changing the power density distribution by welding at different laser beam defocus values resulted in significantly different weld pool shapes. For a given total power

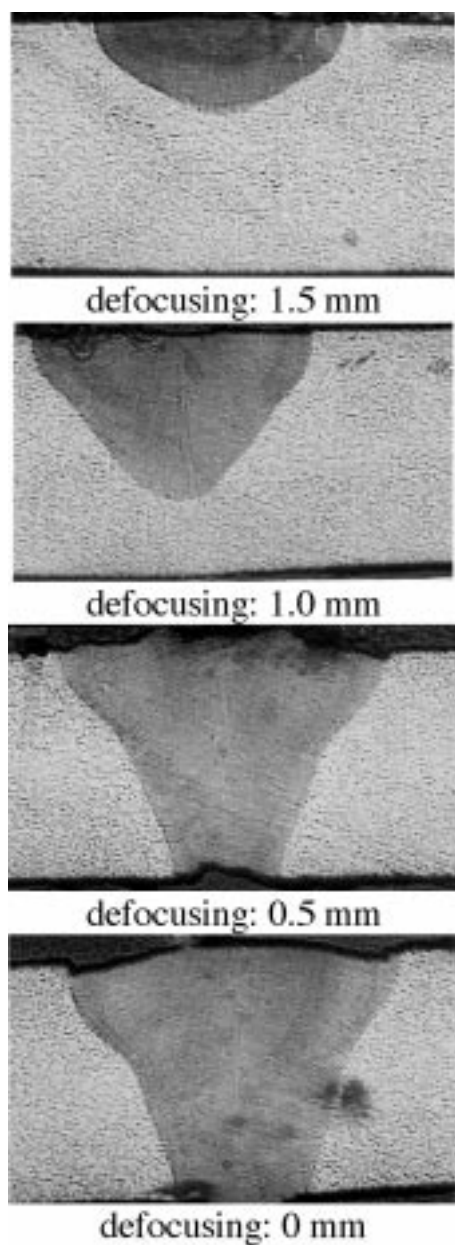
of the heat source, the use of a higher power density heat source results in deeper penetration and enables welding of thicker plates. The experiments²⁴ also indicate that the beam defocusing has to be carefully controlled in order to produce reproducible weld pool geometry during laser welding of aluminium alloys.

Effect of convection on weld pool shape

It is now well known²⁹ that when convection is the dominant mechanism of heat transfer, small amounts of surface active elements, such as sulphur or oxygen in steels, can play an important role in enhancing weld penetration. For example, Fig. 6 shows that the depth of penetration was significantly affected by the concentration of sulphur in steel welds containing 20 and 150 ppm of sulphur and laser welded at a power of 5200 W. However, when convection is not the dominant mechanism of heat transfer, the pool geometries in the two steels are similar as seen from the cross-sections of welds prepared at a laser power of 1900 W. Thus, the effect of sulphur on the weld geometry depended on the laser power and other welding variables. So far, the effect of surface active elements on the shape and size of aluminium weld pools has not been reported in the literature.

Surface tension of aluminium alloys

The values of surface tension as a function of temperature and composition are important in determining the magnitude and direction of the Marangoni stress



5 Cross-sections of Nd-YAG laser welded 1.45 mm thick 5754 aluminium alloy for several beam defocusing values.²⁴ laser power 3.0 kW, welding speed of 150 in min⁻¹

on the weld pool surface. In the absence of surface tension data as a function of temperature and composition, a recourse is to model the surface tension of alloys from fundamentals of thermodynamics and adsorption phenomena. Sahoo *et al.*³⁰ showed that the surface tension of many binary metal surface active solute systems can be adequately modelled on the basis of Gibbs and Langmuir adsorption isotherms and consideration of the surface segregation of the solutes. The dependence of the surface tension of a metal on both temperature and activity of a component is expressed by

$$\sigma = \sigma^0 - A(T - T^0) - 8314T\Gamma_s \times \ln[1 + \kappa a_s \exp(-\Delta H^0/8.314T)] \quad (6)$$

where σ^0 is the surface tension of the pure metal at a

reference temperature T^0 , A is a constant which expresses the variation of surface tension of the pure metal at temperatures above the melting point, Γ_s is the surface excess in saturation, κ is the entropy factor, a_s is the activity of the surface active element in the alloy, and ΔH^0 is the enthalpy of segregation. These models have been successfully used in predicting the surface tensions of ferrous alloys.³¹

The surface tension of pure aluminium decreases with increasing temperature.³² Therefore, the temperature coefficient of the surface tension is negative. However, the true surface tension of molten aluminium is difficult to measure due to the formation of a thin layer of oxide on its surface, even under carefully controlled conditions involving the use of high vacuum or an inert atmosphere.³² Therefore, it is not surprising that wide discrepancies exist in the results obtained by various investigators. The effects of alloying elements on the surface tension³³ are shown in Fig. 7. It is observed that lithium, bismuth, lead, magnesium, antimony, calcium, tin, and, to a lesser extent, silicon, reduce the surface tension of aluminium, whereas germanium, zinc, silver, iron, manganese, and copper have little effect. Though much work has been done on surface tension of binary alloys containing aluminium, very few data are available for commercial and ternary alloys. Goicoechea *et al.*³⁴ measured the surface tension of two ternary aluminium alloys: Al-Si-Mg and Al-Zn-Mg. They showed that the surface tension of these alloys could be obtained from the data for the binaries and pure aluminium

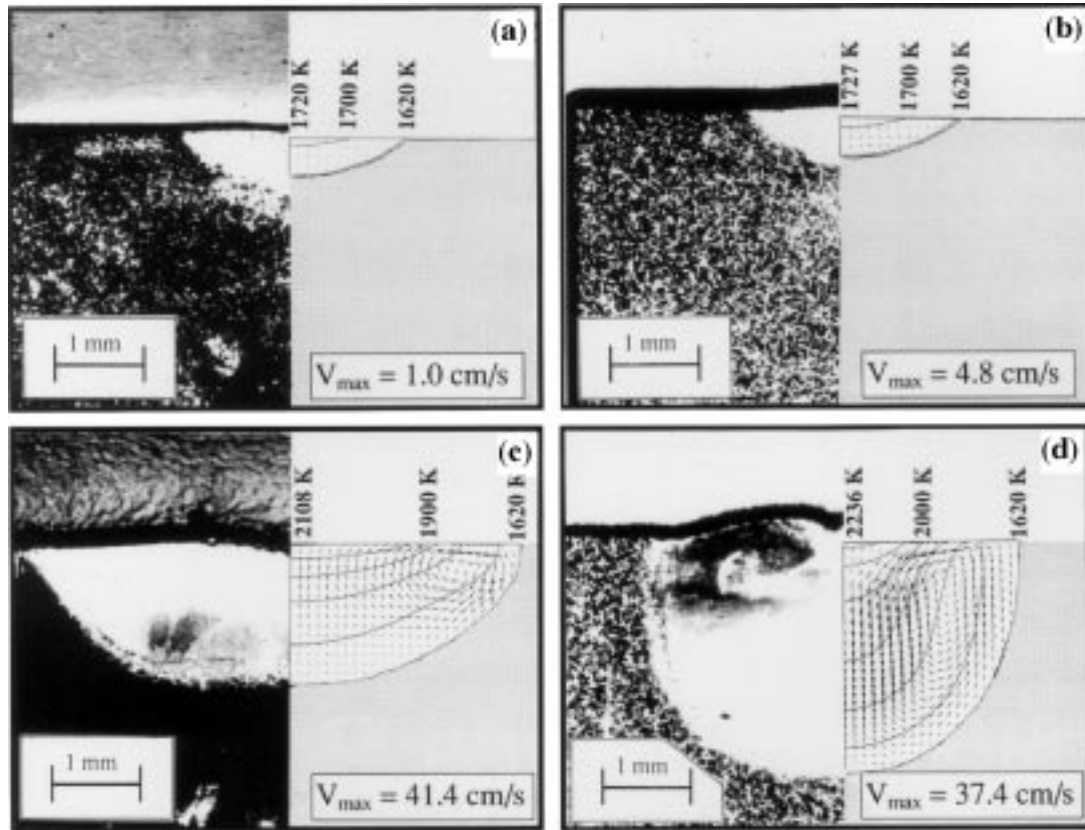
$$X_{\text{Al-A-B}} = X_{\text{Al}} + \Delta X_{\text{Al-A}} + \Delta X_{\text{Al-B}} \quad \dots \quad (7)$$

where A is Si or Zn, B is Mg, $X_{\text{Al-A-B}}$ and X_{Al} are the surface tension of the ternary alloy and pure aluminium respectively, and $X_{\text{Al-A,B}}$ are the increments of the surface tension induced by A or B additions in binary alloys, respectively. This result indicates that the interactions between the constituent elements have little effect on the surface tension of the investigated alloy systems. An appropriate model for the calculation of the surface tension of the aluminium alloys as a function of temperature and composition is not yet available. Such a model is important for accurate calculation of heat transfer and fluid flow in laser welding of aluminium alloys.

Fluid flow and heat transfer in keyhole mode welding

Keyhole mode welding enables the laser beam to penetrate deep into the workpiece, thus achieving deep weld penetration at high welding speed with low heat input. Because of its good seam quality, low distortion, and high productivity, it has found increasing applications in the automotive industry. Much current knowledge on heat and fluid flow in keyhole mode welding has been derived from investigations on both laser and electron beam processing of aluminium and other alloys.

In 1973, Swift-Hook and Gick³⁵ formulated a model of keyhole mode laser welding. They treated the laser beam as a moving line source and obtained a relationship between seam width, absorbed laser power, and welding speed based on heat conduction



a heat containing 20 ppm S, laser power 1900 W; b 150 ppm S, 1900 W; c 20 ppm S, 5200 W; d 150 ppm S, 5200 W

6 Spot weld pool geometries for Bohler S705 high speed steel using CO₂ laser:²⁹ plate thickness 15 mm, irradiation time 5 s, shielding gas 20 L min⁻¹ argon

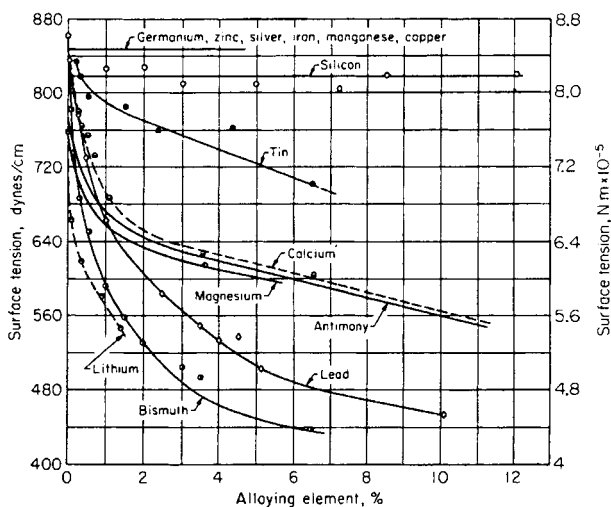
theory. The penetration depth that is usually of significant technical concern could not be calculated since full penetration for all welding conditions was assumed in this model.

Andrews and Atthey³⁶ and Klemens³⁷ proposed models that considered the conditions for the formation of a keyhole. Andrews and Atthey³⁶ obtained the keyhole profile based on the energy balance on the keyhole wall. They showed that the dimensions of the keyhole could be determined from two dimen-

sionless numbers: dimensionless power density $Q = q/(g\rho\rho_g h^2 a)^{1/2}$ and dimensionless surface tension $\tau = T/\rho g a^2$, where q is the power density of the beam, g is the acceleration due to gravity, ρ and ρ_g are the densities of the liquid and vapour respectively, h is the heat of vaporisation, a is the beam radius, and T is the surface tension coefficient. Their calculations showed that the depth of penetration was typically reduced by a factor of about 3 because of the surface tension force. However, the model assumed that all the laser energy was absorbed and used for the vaporisation of the metal. Consequently, heat loss by conduction into the material was neglected. Since these assumptions are not valid in most cases, the model predictions are open to question.

Klemens³⁷ assumed a circular keyhole with vertical walls that was kept open by a balance between forces due to vapour pressure in the keyhole, surface tension, and hydrodynamic pressure in the melt surrounding the keyhole. Absorption of radiation was assumed to take place only by the vapour phase in the keyhole. The temperature distribution was determined from the solution of the heat conduction equation. This model³⁷ was able to calculate the shape of the vapour cavity and of the molten zone and, for this reason, it later served as a basis for the development of several subsequent models.

Mazumder and Steen³⁸ developed a heat transfer model for laser assisted materials processing with a moving Gaussian heat source using a finite difference technique. The model assumed complete absorption



7 Effect of added elements on surface tension of 99.99%Al at 973–1013 K in argon³³

of energy at all locations on the surface where the temperature exceeded the boiling point. The model predictions of weld pool geometry were found to be comparable with the experimental results.

The foregoing models^{35–38} treated only heating of the workpiece. The fluid flow in the molten pool and the convective heat transport were not considered. Dowden and co-workers^{39–42} treated the viscous flow in the weld pool during keyhole mode welding. They^{39,40} assumed a slim cylindrical keyhole of known radius in a molten pool that was almost cylindrical but not concentric to the keyhole due to the movement of the beam. Furthermore, the temperature on the keyhole wall was assumed to be the boiling point. The size of the molten pool was determined from the computed temperature profiles. Only two-dimensional flow with horizontal components was considered. The velocities were obtained by solving Navier–Stokes equations. In subsequent work,^{41,42} it was assumed that all the laser energy was absorbed by the vapour in the keyhole and the keyhole was kept open by equilibrium between forces due to vapour pressure and surface tension. A non-viscous vertical flux of vapour in the keyhole and a viscous vertical flow of molten metal around the keyhole were assumed. With these assumptions, they developed a more comprehensive model that accounted for the vertical variations of keyhole geometry and flow conditions around the keyhole. The model involved the solution of the Navier–Stokes equations, and the equations of conservation of mass and energy.

Kar and Mazumder⁴³ and Mohanty and Mazumder⁴⁴ developed models to predict the weld pool velocities, temperatures, weld pool shape, keyhole depth, and diameter. The models^{43,44} involve the calculations of thermocapillary convection in the weld pool due to the surface tension gradient and the energy balance at the liquid/vapour and solid/liquid interfaces. The calculations showed that the melt velocity in the weld pool could be a higher at higher scanning speed for a given laser power if the laser–vapour interaction became significant. The calculated weld pool geometry was found to compare fairly well with the experimental data. Mohanty and Mazumder⁴⁴ integrated the model into an interactive software tool that can predict molten pool and keyhole geometry for a given set of process conditions.

It is well known that the vertical cross-section of deep penetration welds has a characteristic ‘nail head’ shape. Steen *et al.*⁴⁵ combined a moving point source and a moving line source to describe the laser beam absorption in the keyhole. The temperature distribution obtained from this model yielded a weld pool shape that agreed very well with that found from experimental investigations.

The models described so far did not consider any detailed energy absorption mechanism Herziger *et al.*⁴⁶ presented a detailed theoretical study of the energy absorption processes by the plasma in the keyhole considering inverse Bremsstrahlung. They showed that the penetration increases with laser intensity up to a certain power density. When this power density is exceeded, the weld penetration depth does not increase significantly. They attributed this phenomenon to the shielding effect of the plasma. The

theory provided guidance in choosing effective laser intensities to achieve deep penetration welds. Another important absorption mechanism during keyhole mode welding is multiple Fresnel absorption due to reflections of the beam inside the keyhole.^{47–49} Kar *et al.*⁴⁷ studied the effects of multiple reflections inside the keyhole wall. It was found that multiple reflections led to the formation of deeper and more cylindrical cavities than when multiple reflections were absent. Beck *et al.*⁴⁸ and Kaplan⁴⁹ considered absorption both by plasma and by the Fresnel mechanism due to multiple reflections. Kaplan⁴⁹ found that Fresnel absorption was much higher than plasma absorption during laser welding of iron with laser powers of 4 and 10 kW. It was shown⁴⁹ that the number of multiple reflections was a function of the mean keyhole wall angle. With decreasing penetration depth the keyhole opening angle increased, reducing the average number of multiple reflections and the overall energy absorption.

Many of the existing models assumed a rotational keyhole symmetry and therefore are restricted to low welding speeds. Kaplan⁴⁹ developed a model to calculate the keyhole profile at high welding speeds, using a point by point determination of the energy balance at the keyhole wall. A formula for heat conduction was derived considering a moving line heat source. It was assumed that the laser power absorbed by the keyhole wall balanced the heat loss by conduction into the metal. The different heat conduction conditions at the front wall and at the back wall resulted in an asymmetric profile. The calculated weld pool depth agreed well with the experimental data.

All the above models assumed keyhole wall temperature to be equal to the boiling point of the alloy. However, the force balance on the keyhole wall requires that the temperature of the keyhole wall be higher than the boiling point of the metal.^{50,51} Kroos *et al.*⁵⁰ developed a model in which non-equilibrium evaporation from the keyhole surface, surface tension, and hydrostatic and hydrodynamic pressures in the melt, as well as heat conduction into the workpiece, were considered. The temperature at the keyhole wall and the radius of the keyhole were adjustable parameters in the model. It was found that the temperature at the keyhole wall exceeded the boiling point by approximately 100 K and the keyhole radius was at least 1.7 times the laser radius.

All the models discussed so far assumed the existence of a stable keyhole geometry. However, experimental observations^{52,53} showed the keyhole to be highly unstable during welding. The instability of the keyhole was directly related to the formation of weld defects such as spiking and porosity.⁵³ Some models^{54–56} have been developed to study the dynamic behaviour of the keyhole. Kroos *et al.*⁵⁴ studied the collapse time following sudden laser shut-down and found that the characteristic time constant of the system was $(r_0^3 \rho / \gamma)^{1/2}$, where r_0 is the initial keyhole radius, ρ is the density of the melt, and γ is the surface tension. These results are very important for pulsed laser welding. Klein *et al.*⁵⁵ studied the free oscillations of the keyhole in penetration laser welding. They showed that a keyhole could oscillate in radial, axial, and azimuthal directions. Instabilities

could occur for oscillations with finite amplitudes. Such instabilities could cause weld defects such as spiking or ripple formation. If the absorbed laser power exceeded a threshold value, the oscillations were stable at infinitesimally small amplitudes and the keyhole was more stable under such conditions.

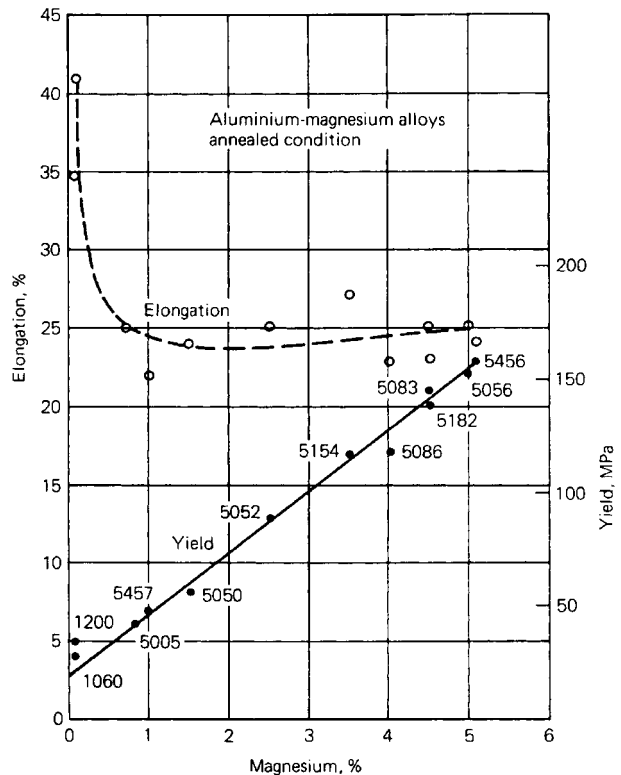
Matsunawa and Semak⁵⁶ developed a model for keyhole propagation during high speed laser welding. A numerical code for the simulation of the front keyhole wall behaviour was developed assuming that only the front part of the keyhole wall was exposed to the laser beam and the recoil pressure exceeded surface tension. The propagation of the keyhole wall inside the sample was assumed to take place by melt expulsion similar to that in laser drilling. The calculations showed that, depending on the processing conditions, the keyhole wall velocity component parallel to the translation velocity vector could be different from the beam translation speed. When this velocity component was higher than the beam translation speed, the formation of the humps on the keyhole wall was computed numerically. They found that the calculated velocity of the melt ejected from the front part of the keyhole into the weld pool could exceed 100 cm s^{-1} at high laser powers.

Reliable models must take into account all the important physical phenomena to be able to explain important features of the process. Because of the complexities of the physical processes during keyhole mode laser welding, development of a unified, comprehensive, mathematical model of temperature and velocity fields in the weld pool is a major task. Efforts are currently under way in several research groups to develop realistic models of keyhole behaviour.

Vaporisation at weld pool surface

Pronounced vaporisation of alloying elements takes place in both keyhole mode and conduction mode welding.^{24,57,58} Since volatile alloying elements such as lithium, magnesium, and zinc have much higher equilibrium vapour pressure than aluminium, they are selectively vaporised during laser welding of aluminium alloys. The 5xxx series alloys usually contain 0.8–5.5% Mg and are primarily strengthened by solid solution of magnesium in the aluminium matrix. Magnesium is also an important constituent of the precipitates in some precipitation strengthened automotive aluminium alloys. The 6xxx series alloys are primarily precipitation strengthened by β' (Mg_2Si) phase. Many 2xxx series alloys containing magnesium are strengthened by the formation of CuMgAl_2 precipitate. The correlation⁵⁹ between the tensile yield, elongation, and magnesium content for some 5xxx series alloys is given in Fig. 8. It is observed that the tensile strengths of these alloys increase linearly with magnesium content. Due to its high vapour pressure and low boiling point, magnesium can be easily vaporised during laser welding, leading to reduction in the tensile strength of the weldments.

Moon and Metzbow⁶⁰ found depletion of magnesium in the fusion zone of laser beam welded 5456 aluminium alloy. In their experiment, a reduction from 5% in the base metal to 4% in the fusion zone was observed. This 20% reduction in the magnesium



8 Correlation between tensile yield, elongation, and magnesium content for some commercial alloys⁵⁹

concentration was considered to be the main reason for the reduced tensile strength of the weldment. Therefore, a reduction in the vaporisation rates of alloying elements during laser welding of aluminium alloys would be desirable.

Factors affecting vaporisation

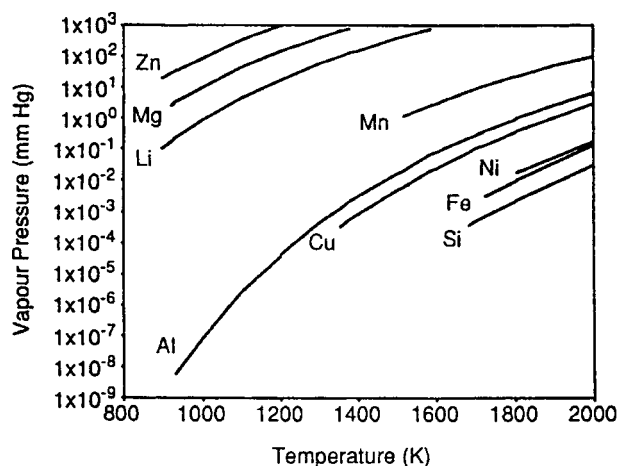
Temperature and composition

A simple model to calculate the vaporisation rate of a pure metal in vacuum is given by the Langmuir equation

$$J = P_0(2\pi MRT)^{-1/2} \dots \dots \dots (8)$$

where J is the vaporisation flux, P_0 is the equilibrium vapour pressure of the vaporising species over the liquid, M is the molecular weight of the vaporising species, R is the gas constant, and T is the temperature. This equation shows that the vaporisation rate is proportional to the equilibrium vapour pressure of the vaporising element. For an alloy, the vaporisation rate of each alloying element can be calculated separately. The overall vaporisation rate of the alloy is the sum of the vaporisation rates of all alloying elements.

Temperature is the most important factor in determining the vaporisation rate because the vapour pressure of a metal is a strong function of temperature. The experimental data⁶¹ for equilibrium vapour pressures of various elements as a function of temperature are given in Fig. 9. It is observed from this figure that at a temperature of 1000 K, magnesium has a vapour pressure of 0.002 atm. However, the vapour pressure of magnesium increases by about 3 orders of magnitude to 2.5 atm when the temperature is increased



9 Equilibrium vapour pressure as function of temperature for various elements⁶¹

to 1500 K. Consequently, the vaporisation rate of magnesium, calculated from the Langmuir equation, increases by three orders of magnitude in this temperature range.

The overall vaporisation rate of aluminium alloys is significantly increased when volatile alloying elements are present. It is observed from Fig. 9 that many important alloying elements in aluminium alloys such as magnesium in 5xxx and 6xxx series alloys and zinc in 7xxx series alloys have much higher vapour pressures than aluminium. For example, at a temperature of 1500 K, the vapour pressures of pure magnesium, zinc, and aluminium are 2.5, 10, and 2×10^{-5} atm respectively. Therefore, even very small additions of magnesium or zinc will significantly increase the overall vaporisation rate of elements from the weld pool.

Block-Bolten and Eagar⁶² studied vaporisation of alloying elements during GTA welding of aluminium alloys. They classified aluminium alloys into the following four groups depending on the composition of vapours over the weld pool:

- (i) zinc vapour dominates in 5xxx series alloys
- (ii) magnesium vapour dominates in 5xxx series alloys
- (iii) roughly equivalent zinc and magnesium vapour pressures are found in 2xxx and 6xxx series alloys
- (iv) alumina vapour dominates in 1xxx series alloys.

Block-Bolten and Eagar⁶² calculated vaporisation rates of the alloying elements using the Langmuir equation. The calculations correctly predicted the dominant metal vapours on weld pools. However, the Langmuir equation overestimates the vaporisation rate at 1 atm pressure because the equation was derived for vaporisation in vacuum where recondensation of the vaporised elements is insignificant. Welding operations are usually carried out at atmospheric pressure where significant amounts of the vaporised elements are recondensed on the workpiece. The recondensation rate must be taken into account in order to obtain realistic predictions of the vaporisation rate. Furthermore, the vapour pressure of aluminium alloys is a strong function of temperature.

Therefore, it is essential to estimate weld pool surface temperature accurately, especially its value near the beam axis where the vaporisation rate is the highest.

Role of plasma

The presence of a plasma may have a significant effect on the vaporisation rate of the weld metal. Collur *et al.*⁶³ and Sahoo *et al.*⁶⁴ studied the effect of plasma on vaporisation rates of iron and copper from isothermal vaporisation experiments. The experiments^{63,64} revealed that the presence of a plasma reduced the vaporisation rate by about 10%, to 50%, for iron and about 60%, to 80%, for copper. The reduction in the vaporisation rates was considered to be consistent with the enhanced condensation of metal vapour due to a space charge effect.⁶⁴ In view of the high mobility of the electrons among the various species in the plasma, the surface of the metal becomes negatively charged since the electrons strike the metal surface at a faster rate than the ions. The attraction between the positively charged ions and the negatively charged surface leads to high condensation rates and consequently, low vaporisation rates in the presence of the plasma.⁶⁴ Experimental data on the effect of plasma on vaporisation of aluminium are not available.

Role of surface active elements

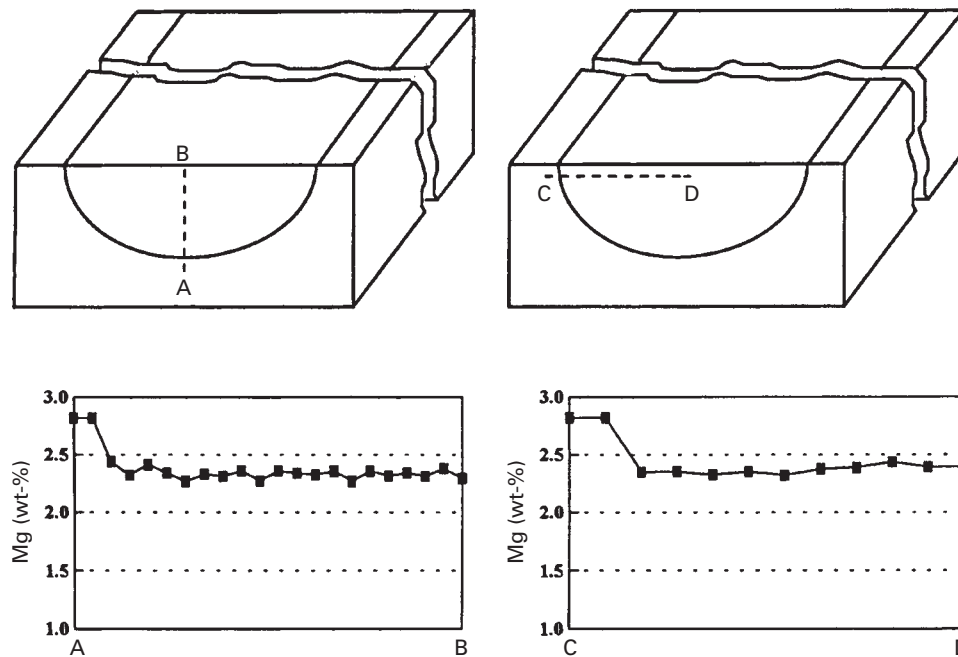
Surface active elements play a mixed role in vaporisation. It is possible that these elements block a portion of the liquid metal surface and reduce the vaporisation rate.⁶³ However, in their isothermal vaporisation experiments, Sahoo *et al.*⁶⁴ found that the presence of surface active elements such as oxygen and sulphur in iron and copper resulted in increased vaporisation rates of the metals. They proposed⁶⁴ that one of the possible opposing effects could be due to interfacial turbulence⁶⁵ caused by the movements of surface active elements from the pool interior to the surface of the liquid. The local movements of the interface increase surface area and therefore increase the rate of vaporisation.

In aluminium alloys, additions of elements such as lithium, bismuth, lead, magnesium, antimony, calcium, and tin, reduce the surface tension of aluminium,³³ as shown in Fig. 7, and so are surface active in aluminium melts. The effects of these elements on vaporisation rate during laser welding of aluminium alloys have yet to be explored.

Mechanism of vaporisation

Collur *et al.*⁶³ studied the mechanism of alloying element vaporisation during conduction mode laser welding. They subdivided the vaporisation process into three steps. The first step involves transport of the alloying elements from the bulk to the surface of the liquid weld pool. Second, vaporisation of the elements takes place at the liquid/vapour interface and, finally, the transport of the vaporised species into the bulk of surrounding gas phase. It was found that the intrinsic vaporisation of alloying elements at the weld pool surface controlled the overall vaporisation rates.

During laser welding, the vigorous circulation of the molten metal driven by the surface tension force greatly enhances the transport of alloying elements



10 Typical magnesium concentration profiles in fusion zone of Nd-YAG laser welded 1.45 mm thick 5754 aluminium alloy:⁶⁶ laser power 3.0 kW, welding speed 250 in min⁻¹

in the weld pool. Calculations showed that the weld pool surface could be renewed about 200 times in the time period required for the laser beam to scan a distance equal to the weld pool width⁶³ during laser welding of pure iron. Since the maximum flow velocity in the weld pool is generally higher during laser welding of aluminium alloys than that of iron,²³ the surface renewal can be assumed to be faster in the aluminium weld pool. In studying alloying element loss during laser welding of 5754 aluminium alloy, Pastor *et al.*⁶⁶ measured the concentration profiles of magnesium along the width and depth of the transverse section of the weld pool, as shown in Fig. 10. The data show that the loss of magnesium was quite pronounced in the fusion zone. There was no concentration variation within the weld pool in macroscale, indicating a vigorous convective mixing in the molten weld metal during welding. Therefore, the transport of alloying elements in the liquid phase does not inhibit the vaporisation. Once an alloying element is transported to the weld pool surface, its vaporisation rate is determined by several variables. These include the surface temperature distribution, local concentrations of the alloying elements, the extent of surface coverage by surface active elements, and other factors such as surface agitation and the modification of the nature of the interface due to the presence of a plasma in the vicinity of the weld pool. The rate of vaporisation at the surface controls the overall loss of elements.⁶³ After the elements are vaporised, their transport from the weld pool surface to the bulk of the gas phase does not slow down the overall vaporisation process.⁶³

The formation of a keyhole during laser welding greatly affects the vaporisation rate and composition change in the weld metal. As the welding changes from conduction mode to keyhole mode, both the volume of the molten weld pool and the vaporisation

rate increase.^{24,57,58} However, the increase in the volume of the molten weld pool is more pronounced than the increase in vaporisation rate. Therefore, the vaporised elements are drawn from a much larger volume of weld pool, resulting in less pronounced composition change in the weld pool during keyhole mode welding.^{24,58}

Miyamoto and Maruo⁵⁷ found that the aspect ratio of the keyhole significantly affected the vaporisation rate during laser welding. The venting of vapour was more difficult and the condensation rate was higher in a slim and long keyhole than in a thick and short keyhole. Therefore, the former resulted in lower vaporisation rate. They claimed that the evaporation flux in conduction mode welding was roughly equal to that in the keyhole mode. Although the recoil force was not measured, they indicated that the recoil force in conduction mode welding was at least as high as that of keyhole mode welding. More work is needed to understand the vaporisation of elements during keyhole mode welding.

Calculation of vaporisation rate and composition change

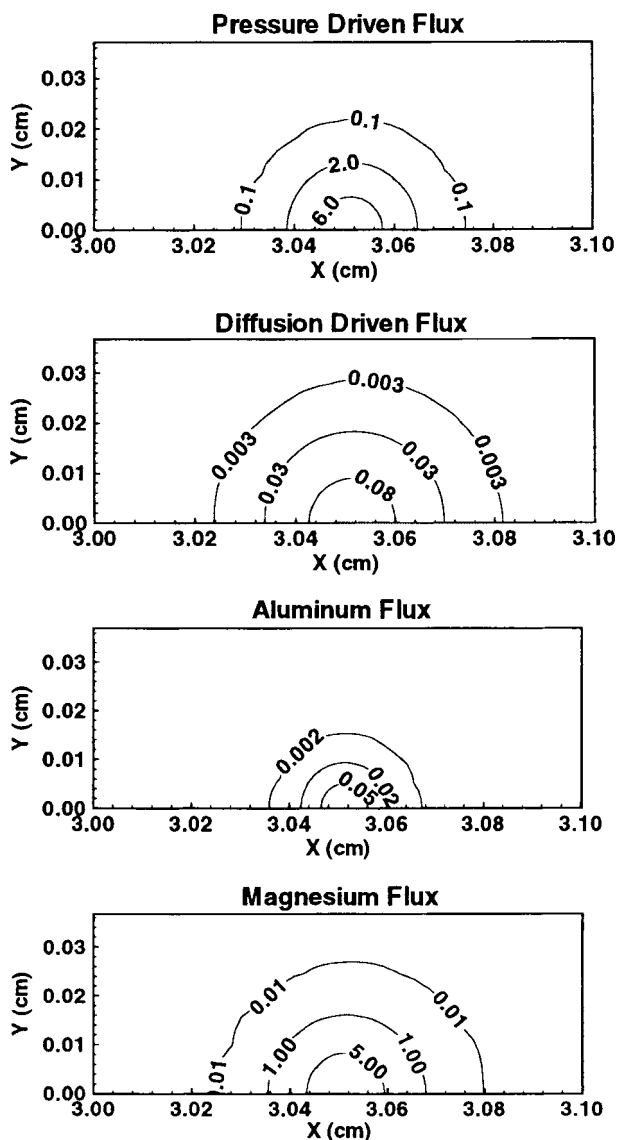
The Langmuir equation can be used to calculate vaporisation rates at very low pressures, where appreciable condensation of the vapour does not take place. Experimental data^{63,64} show that at atmospheric pressure, the vaporisation rate under most fusion welding conditions is 5–10 times lower than the rate predicted by the Langmuir equation. Nevertheless, the equation is useful in calculating the relative vaporisation rates of alloying elements.

DebRoy and co-workers^{67–69} developed a comprehensive mathematical model to describe the vaporisation of pure metals and the loss of alloying elements from stainless steel weld pools. The calculations

involved numerical solution of the equations of conservation of mass, momentum, and translational kinetic energy of the vapour near the weld pool surface. The fluid flow and heat transfer within the molten pool were simulated by the solution of the Navier–Stokes equations, and conservation of energy considerations were used to determine the temperature distribution at the weld pool surface. Heat transfer to the shielding gas and heat loss due to vaporisation of the alloying elements were taken into account in the calculations. The computed weld pool temperature distribution was used for the vaporisation rate calculations.

A key feature of the calculations is the consideration of the pressure gradient driven mass transfer. In laser processing of metals and alloys, the peak temperature at the surface often exceeds the boiling point of the irradiated material. Chan and Mazumder⁷⁰ have reported computed temperatures greater than the boiling points during laser irradiation of aluminium, titanium, and a superalloy. At temperatures higher than the boiling point, the vapour pressure in the vicinity of the weld pool is greater than the ambient pressure. This excess pressure provides a driving force for the vapour to move away from the surface. To include this effect, the velocity distribution functions of the vapour molecules escaping from the weld pool surface at various locations were used in the equations of conservation of mass, momentum, and translational kinetic energy in the gas phase to determine the rates of vaporisation from and the rates of condensation on the weld pool surface.^{67–70} In addition, mass transfer rates due to concentration gradients can be determined using correlation between various dimensionless numbers. The calculated vaporisation rates were in good agreement with the experimentally determined values.

Recently, Zhao and DebRoy⁷¹ extended the above model into three dimensions to include a more rigorous calculation of temperature distribution at the weld pool surface. The model was used to predict the composition change during laser welding of 5182 aluminium alloy. The calculated vapour flux contours are shown in Fig. 11. The predicted vapour flux due to the pressure gradient was much greater than that due to concentration gradient, indicating convection rather than diffusion of vapors contributed most to the overall vaporisation rate. On the other hand, the vapour flux of magnesium was much greater than that of aluminium, resulting in loss of magnesium in the fusion zone. The calculated magnesium loss was in good agreement with the measured change in the composition of the fusion zone. For example, experimental data showed that magnesium loss was about 1.16 wt-% and the model predicted a value of 1.12 wt-% during laser welding of 5182 alloy using a laser power of 3.0 kW, speed of 250 in min⁻¹ (0.11 m s⁻¹), and beam radius of 0.4 mm. The model is useful in predicting composition change during conduction mode laser welding of aluminium alloys. The main lesson to be learned from such agreement is not merely that the predicted vaporisation rates are more accurate than the values obtained from Langmuir equation. In many instances, when an engineer is in search of a theory, simple models such



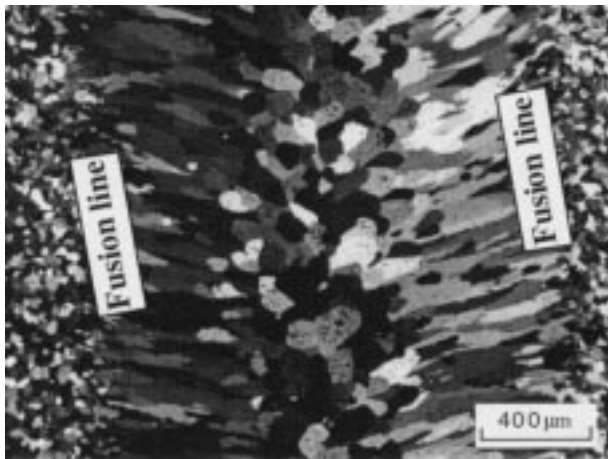
11 Calculated vapour flux contours for Nd-YAG laser welding of 1.0 mm thick 5182 aluminium alloy:⁷¹ laser power 3.0 kW, welding speed 250 in min⁻¹, beam radius 0.40 mm, values on flux contours are in g cm⁻² s⁻¹

as the Langmuir equation can be attractive. The approach adapted in the calculations^{67–69,71} is just the opposite; higher accuracy in the calculated vaporisation rate is achieved by including a more realistic and detailed description of the physical process in welding. However, much work is needed in modelling of vaporisation during laser welding, especially, key-hole mode welding, which is more attractive than conduction mode welding for automotive industry.

Weldment structure and properties

Microstructural features

Laser welded joints are characterised by narrow heat affected zones and fine grained weld zone microstructures. These features result from the low heat input and high cooling rates experienced in laser welds, which are typically made at high travel speeds. The weld zone in fusion welded aluminium is defined⁷²



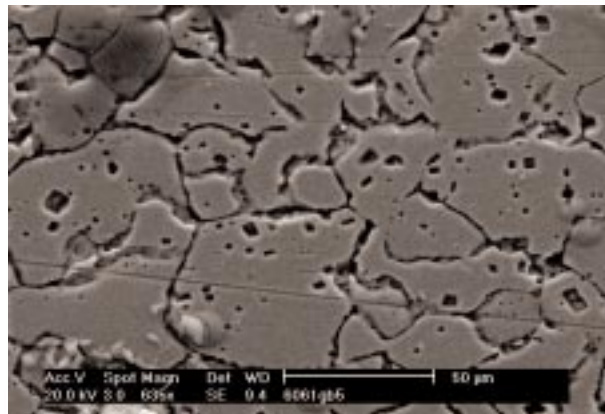
12 Typical microstructure of laser welded 5754-O aluminium alloy using 3 kW cw Nd-YAG laser at welding speed of 200 in min^{-1} (Ref. 76)

as consisting of the fusion zone, the partially melted zone, and the heat affected zone. While the partially melted zone and the heat affected zone are generally narrower and less distinct than those in processes such as gas tungsten arc welding with higher heat input,⁷² the above definition is used in the present review to describe the findings of microstructural characterisation studies in laser beam welding of automotive aluminium alloys. The automotive aluminium alloys for which published information is available on microstructures of laser welds include:^{60,72-81} 5083, 5086, 5251, 5456, 5754, 6013, 6061, 6063, 6082, and 6111. The effects of both CO₂ and Nd-YAG laser welding have been investigated.

Fusion zone

The fusion zone of both 5xxx and 6xxx series laser welded alloys consists primarily of fine columnar dendrites originating from the fusion line and equiaxed grains existing in the centre of the fusion zone.⁷²⁻⁷⁸ Figure 12 shows the typical microstructures in the fusion zone of laser welded 5754-O alloy.⁷⁶ Weld defects such as solidification cracking and porosity may occur in the fusion zone. Modification of the weld metal composition through use of filler metal and proper selection of welding parameters are essential to avoid cracking and porosity.

Laser welded 5xxx alloys In one of the earlier studies of the laser welding of aluminium alloys, Moon and Metzbow⁶⁰ investigated laser welding of 0.5 in thick 5456 alloy. Although material of this thickness is of little interest in automotive applications, their observations about microstructure are consistent with work by others on thinner sections. A fine grained structure in the fusion zone was observed. In addition, depletion of magnesium and removal of precipitates such as Mg₂Si and (Fe,Mn)Al₆, were noted. While the depletion of magnesium is harmful to the mechanical properties of the welds, the refined structure after the removal of the precipitates was considered⁶⁰ to contribute to the increased toughness of the welds. In an investigation of laser welding of aluminium alloys for automotive application, Ramasamy and Albright⁷⁶ compared welding of 1.6 mm thick 5754-O alloy with



13 Microstructure showing equiaxed grain structure along centre of laser weld in 6061 aluminium alloy⁸¹

CO₂ and Nd-YAG lasers using power of 5 and 3 kW respectively. They found the weld metal microstructure in both cases to be fine cellular dendritic, with equiaxed grains in the middle of the weld. The volume of equiaxed grains increased with increasing travel speed. Venkat *et al.*⁷⁷ investigated CO₂ laser welding of 1.6 mm thick 5754-O alloy using a power of 3 kW and travel speeds of up to 400 in min^{-1} (0.17 m s^{-1}). A fine cellular dendritic structure was commonly observed in the fusion zone. Only occasionally were the equiaxed grains observed near the weld centreline at high welding speeds.

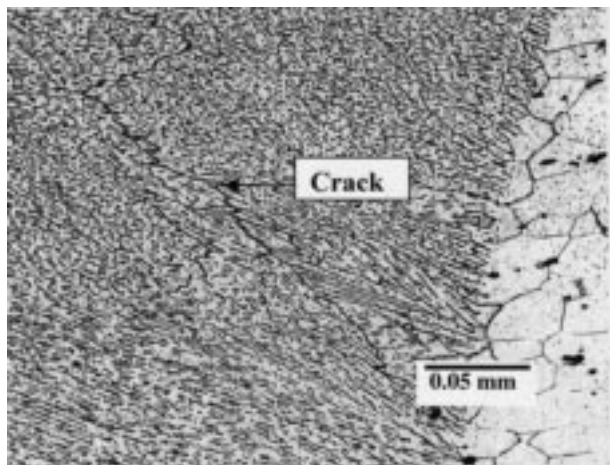
Solidification cracking was not reported in continuous wave laser welding of 5xxx series alloys.^{60,73,76-79} However, Cieslak and Fuerschbach⁷⁹ observed solidification cracking during pulsed Nd-YAG laser welding of 5456 alloy and suggested that the rapidly developing thermal strains due to the high cooling rates were responsible for the cracking.

Laser welded 6xxx alloys Laser welded 6xxx series alloys^{72-75,77,78,81} demonstrated fine cellular dendrite structures that originated from the fusion line and extended to the centre of the fusion zone. For these alloys equiaxed grains were consistently observed by various investigators^{72-75,77,78,81} under diverse welding conditions. Both CO₂ and Nd-YAG lasers were used to weld plates of thickness in the range 1–10 mm, with laser power from 2 to 7 kW and welding speeds of 8–168 mm s^{-1} . Figure 13 is an example of equiaxed grain structure along the centre of the fusion zone in laser welded 6061 alloy.⁸¹

Solidification cracking has been observed^{74,75,77} during autogenous laser welding of 6xxx alloys. Figure 14 shows solidification cracking in the fusion zone of laser welded 6111-T4 alloy.⁷⁵ The cracking was more pronounced at high welding speeds due to the high cooling rates.^{74,75} The mechanism and control of solidification cracking will be discussed below.

Partially melted zone

The partially melted zone has temperatures between the liquidus and eutectic temperature of the alloy. Therefore, the low melting point eutectic phases which commonly exist at the grain boundaries of recrystallised grains remelt during laser welding. Liquation cracking may occur along these weakened grain



14 Solidification cracking along cellular dendritic grain boundary of 6111-T4 aluminium alloy welded using 3 kW CO₂ laser at welding speed of 400 in min⁻¹ (Ref. 75)

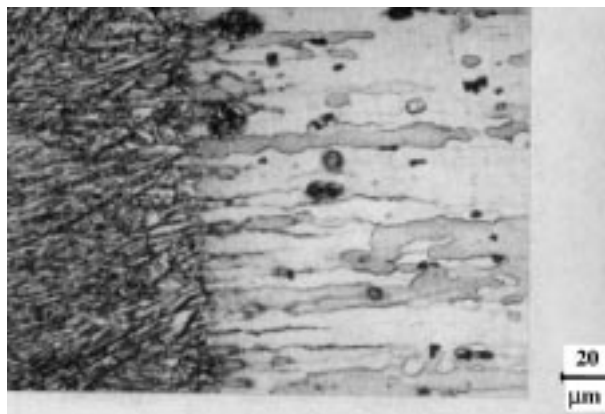
boundaries. The partially melted zone in laser welded aluminium alloys is generally narrow and is only one or two grains wide.^{72,75,77} Guiterrez *et al.*⁷² observed that even when the grain size of the base metal was very large and high laser power was used in welding of 6013 aluminium alloy extrusions, only a small amount of liquid was formed near the fusion line, as shown in Fig. 15. Therefore, liquation cracking is not a major concern in the laser welding of automotive aluminium alloys.

Heat affected zone

The heat affected zone has a maximum temperature below the eutectic temperature of the alloy and no melting occurs in this region. However, many solid phase reactions such as grain growth and precipitate coarsening occur in this region and affect the properties of the material. For welding of automotive aluminium alloys, softening is a prime concern in the heat affected zone. Softening occurs due to grain growth or loss of strain hardened structure for non-heat treatable aluminium alloys such as the 5xxx series.⁶⁰ For heat treatable aluminium alloys such as 6xxx series alloys, the dissolution of the strengthening β'' phase (semicoherent rods of Mg₂Si) and formation and growth of non-strengthening β' precipitates (semicoherent needles of Mg₂Si) cause softening in the heat affected zone.⁷² The high power density and high speed in laser welding cause steep temperature gradient and high cooling rate in the weld metal. Consequently, the heat affected zones in laser welds are narrower than in other fusion welding processes with lower power densities such as gas tungsten arc welding and gas metal arc welding.⁷² Therefore, the softened region in laser welded aluminium alloys is smaller than those in the latter welds.

Role of filler metals

Many automotive aluminium alloys, such as 6xxx series alloys, are susceptible to solidification cracking. The cracking susceptibility is directly related to the compositions of the alloys. The use of filler materials can modify the composition of the fusion zone so that the compositions which are susceptible to solidi-

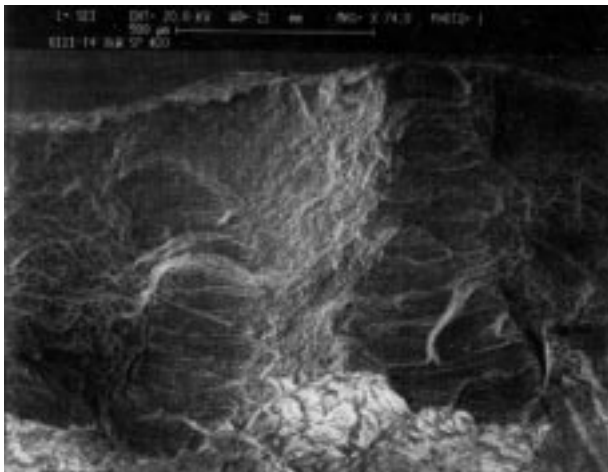


15 Photomicrograph showing evidence of liquation at grain boundaries during welding of 6013-T6 aluminium alloy using 7 kW CO₂ laser at 100 mm s⁻¹ travel speed⁷²

fication cracking can be avoided in the welding of these alloys. An appropriate filler metal may also compensate for the loss of volatile alloying elements.

Katsuna *et al.*⁷⁸ studied the addition of 4043-WY and 4047-WY filler wires during CO₂ laser welding of 4 mm thick 6063 plates at a power of 4 kW and speed of 3 m min⁻¹. As with autogenous welds, the microstructure of the weld zone consisted mainly of cellular dendrites with a small number of equiaxed grains at the top of the fusion zone centreline. The use of 4043 filler metal at a feed rate of 50 mm min⁻¹ was found to reduce the degree of solidification cracking, but microcracks were still observed at the bottom of the weld. Using electron probe microanalysis (EPMA), the concentration of silicon in the welds was found to be inhomogeneous at the macroscale and to decrease from about 2% at the top of the welds to about 1% at the bottom. The inhomogeneity of the silicon distribution was attributed to the rapid solidification which prevented sufficient mixing of the filler metal and the base metal at the bottom of the weld pool.⁷⁸ Increasing the wire feed rate to 100 mm min⁻¹ and using 4047 filler metal containing higher silicon content resulted in a silicon concentration of 3% at the bottom of the welds and prevented crack formation. Therefore, maintaining the concentration of silicon in 6xxx series alloys above a certain critical level is essential to avoid solidification cracking. The relationship between the solidification cracking susceptibility and the composition of aluminium alloys will be discussed below.

Starzer *et al.*⁸² also studied the use of filler materials in the laser welding of 6xxx series alloys. They added filler wire and powders during CO₂ laser welding of 4 mm thick 6060 and 6080 alloys. In their work, silicon and Al-12Si powders with particle sizes of 40 and 150 μ m respectively, were fed into the interaction zone of beam and workpiece during welding of 6060-T6 alloy. Although the powder additions were found to reduce crack susceptibility by increasing the silicon content of the fusion zone, inhomogeneous mixing at travel speeds above 0.5 m min⁻¹, high porosity, and low powder efficiency were identified as problems requiring further investigation. The effects of feeding 4043 and 4047 wires were examined during



16 Fractograph showing two distinct fracture modes in different regions of tensile specimen of CO₂ laser welded 6111-T4 aluminium alloy tested in longitudinal direction:⁷⁷ ductile fracture at centre of weld metal and fracture characterised by large facets near fusion boundary

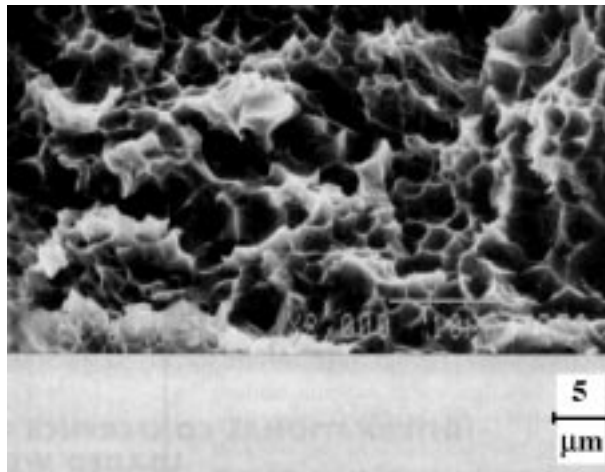
welding of 6060-T4 and 6082-T6 alloys. Filler wire additions were also found to increase weld zone silicon contents and reduce fusion zone crack susceptibility. Homogeneous mixing could be obtained at weld speeds of up to 1.3 m min⁻¹. Starzer *et al.*⁸² concluded that the filler wires are potentially useful for production applications.

Fractography

Fractographic studies reveal information about the ductility of a material and fracture mechanism. Several investigators have examined the fracture surfaces of laser welded aluminium alloy tensile^{72,75-77} and impact⁶⁰ specimens. Ramasamy and Albright⁷⁵ and Venkat *et al.*⁷⁷ observed two distinct fracture modes in different regions of the tensile specimens of CO₂ and Nd-YAG laser welds of 6111-T4 alloy tested in the longitudinal direction, as shown in Fig. 16. The base metal and the centre of the fusion zone displayed a ductile dimple type of fracture, with the width of the ductile dimple rupture zone in the centre of the weld decreasing as the travel speed increased.⁷⁵ The fractured surface of the fusion zone adjacent to the fusion boundary had a different appearance, with large faceted surfaces, possibly associated with the large columnar grains of the fusion zone. However, Guitierrez *et al.*⁷² observed ductile fracture in the fusion zone of laser welded 6013-T6 alloy, as shown in Fig. 17.

The fracture surface of laser welded 5754-O alloy indicated a failure caused by dimple rupture⁷⁶ or microvoid coalescence⁷⁷ over the entire weld zone. These types of failure are commonly observed in the ductile rupture of materials. Moon and Metzbowler⁶⁰ conducted dynamic tear testing and also observed ductile fracture in laser welded 5456 alloy.

Detailed microstructural studies using optical microscopy, SEM, STEM/EDS, and TEM have been done on pulsed Nd-YAG laser welded rapidly solidified/powder metallurgy Al-8Fe-2Mo alloy.⁸⁰



17 Scanning electron micrograph of typical fracture surface of laser welded 6013-T6 aluminium alloy tensile specimen that fractured in fusion zone⁷²

Such studies provided significant insight in the evolution of microstructure in the weld and its relation with the weld properties. However, much of the microstructural investigation on laser welded automotive aluminium alloys has been limited to optical microscopy and SEM fractography. More detailed microstructural analyses are needed to address the issues related to hot cracking susceptibility and joining of dissimilar alloys.

Effect of welding on mechanical properties

Configuration of the joint (lap joint, butt joint, etc.) and the presence of undercuts, humping, cracking, porosity, and other defects affect the mechanical properties of the joints. During laser welding of automotive aluminium alloys, the ultimate strength of the weld is often reduced due to poor root quality and/or undercutting.⁸³⁻⁸⁵ The use of 4047 filler alloy was necessary for 2xxx and 6xxx series alloys to eliminate solidification cracking and undercutting.⁸³⁻⁸⁵ While autogenous welding of 5xxx series alloys could be performed without producing solidification cracking, the use of 5554 filler alloy eliminated undercutting and increased the tensile strength and elongation of the welds.⁸³⁻⁸⁶ However, the yield strength was decreased by the use of the filler material in the welding of 5xxx series alloys.⁸³⁻⁹⁶

Important changes occur in different regions of the weld. The fusion zone structure is generally very different from that of the base metal. Selective vaporisation of volatile constituents from the fusion zone changes the composition of the alloy and may degrade the mechanical properties of the weld metal.^{60,80,87} In the partially melted zone and heat affected zone, the thermal cycles affect the original structure and mechanical properties of the alloy. Particularly, over-aging the heat treatable alloys causes loss of precipitation hardening and annealing of non-heat treatable alloys causes loss of work hardening. While the loss of strengthening in non-heat treatable alloys is irreversible, post-weld aging of the 6xxx alloys slightly

increased the tensile strength of the joints and significantly reduced elongation.^{83–85}

Mechanical characterisation

Mechanical properties of several laser welded automotive aluminium alloys have been reported in the literature.^{60,83–88} These include: 2008, 2010, 5083, 5182, 5251, 5454, 5754, 6009, 6060, 6061, 6082, and 6111. The thickness of the material ranged from 1.0 mm to 2.5 mm. Carbon dioxide lasers with powers in the range^{83–85,87,88} 4–6.8 kW and Nd-YAG lasers with powers in the range^{86–88} 2–3 kW were used. The welding speeds varied from 0.9 to 7.0 m min⁻¹, depending on the thickness of the material and the laser power. Both butt and lap welds were evaluated. In many cases, welds of the heat treatable 2xxx and 6xxx alloys were produced with 4047 filler alloy additions to avoid cracking.^{83–85} Welds of 5xxx alloys were produced both autogenously^{83–88} and with 5554 filler alloy additions^{83–85,88} to compensate for magnesium loss during welding. The mechanical property tests carried out included tensile tests,^{83–88} guided bend tests,^{83–85} limiting dome height tests,^{83–87} and dynamic tear tests⁶⁰ for butt welds; tensile tests, tension shear tests, and peel tests for lap welds;^{83–85} and axial fatigue tests for both butt and lap welds.^{83–85} The results are discussed in the following sections.

Tensile properties

Tensile specimens cut from autogenous butt welded 5xxx series alloys failed in the fusion zone.^{83–87} The tensile strengths of the welds were about 90% of those in the base metals^{86,87} with higher strength being associated with higher magnesium content.⁸⁷ Butt welding of 5xxx series alloys with 5554 filler alloy additions^{83–85} eliminated undercutting in the welds and increased the tensile strength and elongation of the welds. In some cases, failure occurred in the base metal.

For autogenous butt welding of 6xxx series alloys,⁸⁷ tensile specimens failed in the heat affected zone. The tensile strengths of the welds were about 60% those of the base metals. Addition of 4047 filler alloy during butt welding of 6xxx and 2xxx series alloys produced welds with strengths comparable to the lowest values in the range of the base metal strength values.^{83–85} Post-weld aging treatment on these welds significantly increased the hardness of the heat affected zone due to GP zone recovery. However, the hardness of the fusion zone did not change significantly. The composition of this region was very different from that of the base metal due to the addition of the filler alloy. As a result, a moderate increase in tensile strength and a significant reduction in elongation were observed when the welds were examined in post-weld aged conditions.^{83–85} Lap joints generally resulted in lower joint efficiencies than butt joints.⁸⁷ The tensile strengths of the lap joints were 34–70% of the base metal values.

Formability and fracture toughness

Limiting dome height (or bulge height) tests showed that laser welding decreased the formability of all alloys^{83–87} due to stress concentrations arising from the inhomogeneous strength across the weld^{83–85} or imperfect fusion zone geometry.⁸⁶ For laser welds with filler alloy additions,^{83–85} the 5xxx series alloys

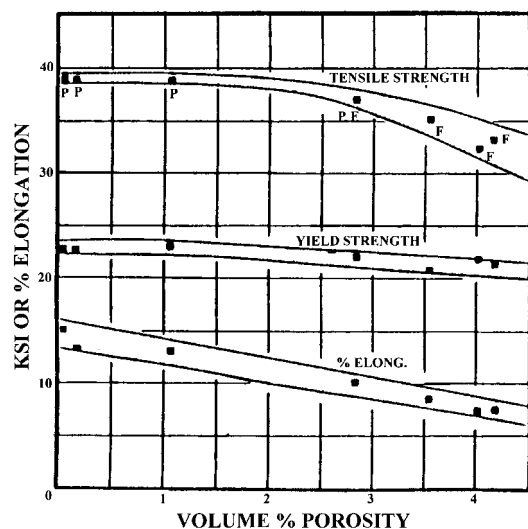
had a higher ratio of average dome height of welds to that of the base metal than the 2xxx or 6xxx series alloys. The laser welded 5754-O alloy with 5554 filler alloy additions exhibited formability of about 90% that of the base metal. Fractures during limiting dome height tests in the 2xxx and 6xxx series alloys were initiated within the fusion zone where the hardness was the lowest. In contrast, the 5xxx series alloys developed slightly higher strength in the fusion zone than in the heat affected zone. The gradual change in strength of the 5xxx series alloys, indicated from the hardness profiles across the welds, resulted in more uniform straining and better formability. For autogenous laser welds,^{86,87} a formability of 70% of the base metal value was obtained in autogenous laser welded 5754-O alloy.⁸⁶ Bulge heights of 25–30 mm and 10–15 mm were achieved in the 5xxx and 6xxx series alloys respectively.⁸⁷

Dynamic tear tests⁶⁰ in autogenous welds of 5456 alloy showed that the toughness was greater for the weld bead than for the base metal and fracture took place by microvoid coalescence. The increased toughness of the weld bead was considered to be due to the reduction of precipitates such as Mg₂Si and (Fe,Mn)Al₆ during laser welding.⁶⁰

Other properties

Other important mechanical properties of laser automotive alloys include fatigue strength and peel strength. Joint configuration and fusion zone geometry greatly affect the weld fatigue strength. Butt welds are found to have better fatigue performance than lap welds owing to higher stress concentration in the lap welds.^{83–85} In a production application, however, consideration would have to be given to the greater difficulties involved in achieving uniformly high quality in butt welds, and the possible effects on the uniformity of mechanical properties in a large number of joints. Peel tests were used to determine the strength of lap welds under peel conditions. The non-heat treatable 5xxx series alloys exhibited nearly 2.5 times higher peel strength than the heat treatable materials.⁸³ The large difference in peel strength between heat treatable and non-heat treatable alloys is not well understood.⁸³ Since peel strength is a key parameter used by the automotive industry, this issue should be investigated further.

Rapp *et al.*⁸⁸ showed that the static strength of laser welded aluminium alloy butt joints was higher than that of similar joints welded using gas tungsten or gas metal arc welding. The higher strength was attributed to the relatively low heat input of the laser welding process. They demonstrated the feasibility of producing tailored blanks with different sheet thickness from dissimilar automotive aluminium alloys using laser butt welding. The static strength of butt welded sheets of different materials (6009-T4 to 5182-O) showed values at least as good as the weaker of the two materials. Furthermore, the dynamic strengths of the dissimilar alloy tailored blanks (1.25/2.25 and 1.25/1.25 mm 6009-T4/5182-O) in welded condition were similar to the values for welded 1.25 mm thick sheets of the same materials.⁸⁸ Therefore, expanded use of lasers for the welding of automotive aluminium alloys appears promising in this application.



18 Effect of weld porosity on tension test performance.⁸⁹ P = passed bend test, F = failed bend test; 1 ksi = 6.895 MPa

Porosity

Porosity is a common problem in laser welded aluminium alloys. The detrimental effect of porosity on mechanical properties of aluminium welds has been documented in the literature.^{89,90} Ashton and Wesley⁸⁹ studied the effects of weld porosity on the tensile and bend test performances of 5086–H116 alloy welded with 5356 electrodes. Their results are shown in Fig. 18. They found that weld porosity is detrimental to the static tensile properties and bend ductility of the welds. The elongation can be reduced by 50% from its highest level as the porosity level is increased to 4 VPP (volume percent porosity). The yield strength is reduced only slightly by porosity levels up to about 4 VPP. The tensile strength is unaffected by a small amount of porosity, but drops below 35 ksi (241 MPa) when the porosity is higher than 3.6 VPP. It is also noted that when the porosity level is higher than 2.5 VPP, the reduction in tensile strength is more severe; this may exceed the effect caused by reduction in cross-sectional area due to porosity.

Kato⁹⁰ tested the tensile strength of 5083–O specimens with two holes drilled transverse to the direction of load to simulate porosity. It was found that when the distance between neighbouring holes was greater than the hole diameter, the tensile strength decreased linearly with the increase in the hole diameter, irrespective of the hole interval. On the other hand, when the hole interval was smaller than the hole diameter, the tensile strength was further reduced. Kato⁹⁰ proposed that when the pores were near each other, the zone between them carried hardly any load, resulting in further reduction in effective loading cross-sectional area of the specimen. This may explain the accelerated reduction in tensile strength at high porosity levels, where both the porosity and the intervals between the pores contribute to reducing the effective loading area.

There are at least two possible causes for porosity formation.⁹¹ One is based on the absorption and subsequent entrapment of the ambient gases during

the welding process. For example, all aluminium alloys are prone to hydrogen induced weld metal porosity. Another is based on the entrapment of gas bubbles due to imperfect collapse of the keyhole generated by the high intensity laser beam.

Porosity due to absorption and entrapment of gases

Depending on the composition of the gases near the weld pool, the molten aluminium alloy in the weld pool may absorb different amounts of ambient gases such as oxygen, nitrogen, and hydrogen. In principle, these gases may be released during subsequent cooling because of their reduced solubility at lower temperatures. If the released gases fail to escape from the weld pool before solidification, they may be entrapped in the fusion zone, resulting in porosity. This type of porosity arises due to the large decrease in solubility of the gases in solid aluminium alloys. The role of these gases in the formation of porosity in aluminium welds is examined in the following section.

Solubility of oxygen

The oxides of aluminium, magnesium, manganese, and silicon are highly stable at the temperatures prevailing in the weld pool and the solubility of oxygen in aluminium alloys at these temperatures is very small and difficult to measure. Since the oxides formed in aluminium alloys are stable, molecular oxygen is unlikely to be formed by decomposition of these oxides during laser beam welding. Therefore oxygen is highly unlikely to be the cause of porosity in laser beam welding of aluminium alloys.

Solubility of nitrogen

The solubility⁹² of nitrogen in aluminium is less than 1×10^{-11} at.-% at about 933 K. During laser beam welding, nitrogen is absorbed in the molten aluminium alloy by the reaction



$$\Delta G_1^\circ = -78\,170 + 27.61T \text{ cal mol}^{-1} \text{ (Ref. 93)}$$

$$\dots \quad (10)$$

(1 cal = 4.18 J). In the presence of plasma over the weld pool, the possible reactions are

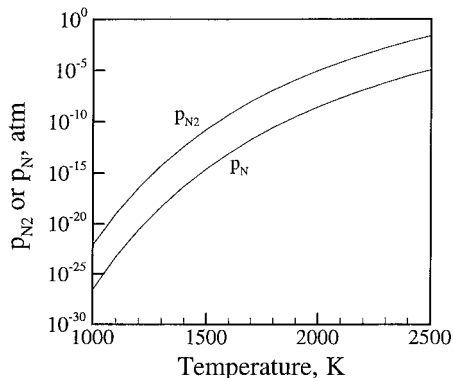


$$\Delta G_3^\circ = 865\,960 - 15.659T \text{ cal mol}^{-1} \text{ (Ref. 94)} \quad (12)$$



$$\Delta G_5^\circ = \Delta G_1^\circ - \Delta G_3^\circ \quad \dots \quad (14)$$

The equilibrium partial pressures of N_2 and N(g) according to equations (9) and (14) indicate that very low partial pressures of these gases are required to form AlN and reflect the tendency for AlN formation. From the standard free energies for the formation of AlN, the partial pressures of N_2 and N(g) in equilibrium with AlN at the temperatures of interest in welding aluminium alloys can be calculated. The calculated values are plotted in Fig. 19 and they show that AlN can be formed at very low N_2 or N(g) partial pressures. It is also seen that the equilibrium partial pressure of N(g) is much lower than that of N_2 at any temperature indicating that AlN can be more readily formed in the presence of atomic nitro-



19 Calculated equilibrium partial pressure of diatomic nitrogen and monatomic nitrogen in forming aluminium nitride, as function of temperature

gen gas. The increasing values of the partial pressures of both N(g) and N₂ show the greater stability of AlN at lower temperatures. Since nitrogen is absorbed by the molten pool mainly by the formation of AlN which is more stable at lower temperatures, nitrogen as the cause of porosity during laser beam welding of aluminium alloys can be ruled out. Katayama⁹⁵ reported that porosity was reduced in laser welding of aluminium alloys when nitrogen was used as the shielding gas. He proposed that the formation of nitrides on the molten pool surface inhibited the absorption of hydrogen by the molten pool.⁹⁵ A comprehensive study of the role of nitrides on hydrogen absorption in molten aluminium during welding still remains to be undertaken.

Solubility of hydrogen

Hydrogen has significant solubility in aluminium and is generally considered to be the primary cause of porosity during the welding of aluminium alloys. The measured values of hydrogen solubility in pure aluminium vary according to the data furnished by different investigators.⁹⁶⁻¹⁰⁴ Among the data considered reliable are those by Ransley and Neufeld⁹⁶ who found that the solubility of hydrogen in liquid aluminium can be expressed by the equation

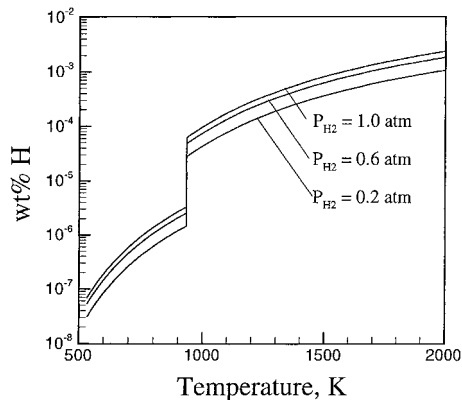
$$\log S = -(2760/T) + \frac{1}{2} \log P + 1.356 \quad \dots (15)$$

and that in solid aluminium by

$$\log S = -(2080/T) + \frac{1}{2} \log P - 0.652 \quad \dots (16)$$

where *S* is the solubility of hydrogen (mL/100 g Al) measured at 273 K and 760 torr, *T* is the temperature (K), and *P* is the partial pressure of hydrogen (torr; 1 torr = 0.133 mbar). The calculated hydrogen solubilities in solid and liquid aluminium at three different H₂ partial pressures are given in Fig. 20. The plot shows that the solubility of hydrogen in aluminium decreases with decreasing temperature and that its solubility in liquid aluminium is about 20 times higher than that in solid aluminium at the melting point of 933 K. This explains why aluminium and its alloys are highly susceptible to hydrogen porosity during welding.

An additional factor to be considered in laser beam welding is that a plasma phase containing the atomic



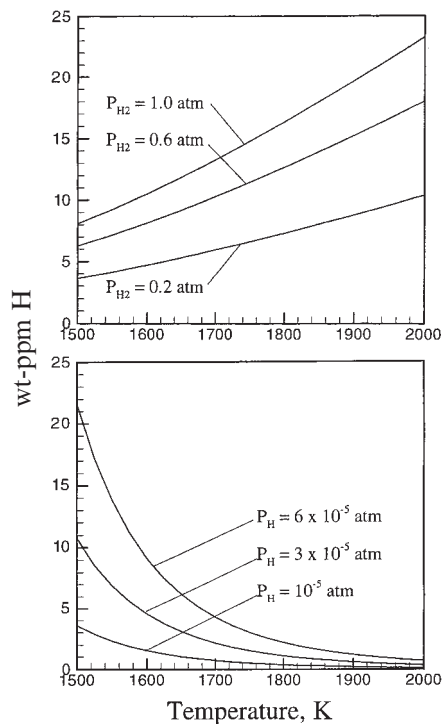
20 Calculated hydrogen solubility in aluminium, based on results of Ransley and Neufeld⁹⁶

gaseous species can be formed over the weld pool. In the presence of atomic hydrogen the solubility of hydrogen in liquid aluminium can be greatly enhanced. Using the data⁹⁶ in equation (15) and the standard free energy of formation¹⁰⁵ of atomic hydrogen gas in equation (18), the solubility of hydrogen in liquid aluminium in environments of molecular and atomic hydrogen can be calculated

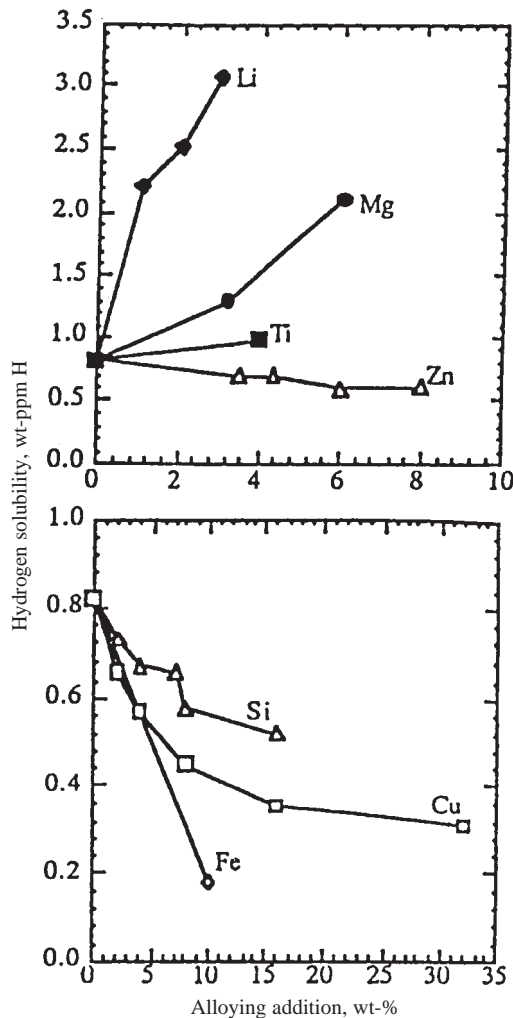


$$\Delta G_0^\circ = 53\,550 - 14.4T \text{ cal mol}^{-1} \text{ (Ref. 105)} \quad (18)$$

The calculated results are plotted in Fig. 21. It is seen that the solubility of hydrogen in aluminium at 1500 K is about 8 wt-ppm in 1 atm diatomic hydrogen environment and the solubility is increased to about 11 wt-ppm at only 3×10^{-5} atm partial pressure of monatomic hydrogen.



21 Calculated hydrogen solubility in aluminium in environments of diatomic hydrogen and monatomic hydrogen



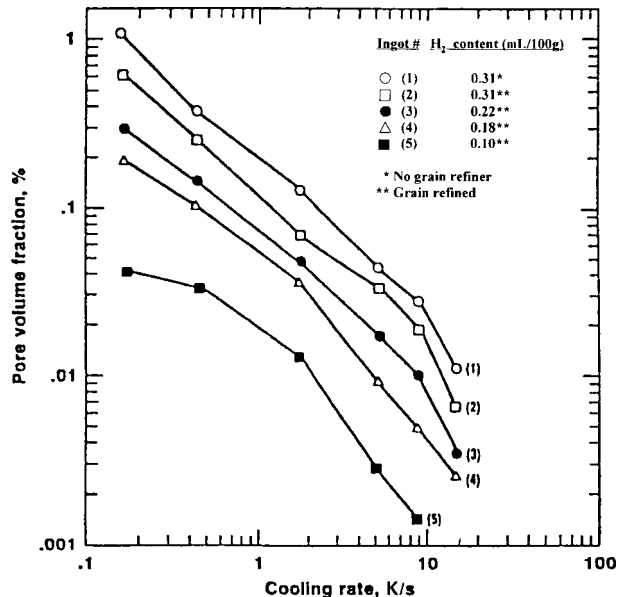
22 Effect of alloying elements on solubility of hydrogen in liquid aluminium at 973 K and 1 atm partial pressure of hydrogen¹⁰⁶

Effect of alloying elements on the solubility of hydrogen in aluminium

Anyalebechi¹⁰⁶ has reviewed the effect of alloying elements on hydrogen solubility in liquid aluminium and the results are shown in Fig. 22. The presence of lithium, magnesium, and titanium increases the solubility of hydrogen in liquid aluminium whereas zinc, silicon, copper, and iron reduce it. This behaviour can be attributed to the strong attractive interactions between hydrogen and lithium, magnesium, and titanium on the one hand and the strong bonding of aluminium atoms to zinc, silicon, copper, and iron on the other.

Nucleation and growth of hydrogen bubbles in weld metal

As noted above, the solubility of hydrogen in liquid aluminium decreases with temperature and is about 20 times higher in liquid aluminium than in the solid near the melting point. Therefore, the molten aluminium weld pool becomes highly supersaturated with absorbed hydrogen in the subsequent cooling process. To reduce the supersaturation, hydrogen bubbles form by a process of nucleation and growth. However, the high surface tension of liquid aluminium does not



23 Pore volume fraction as function of cooling rate in Al-4.7Mg alloy¹⁰⁷

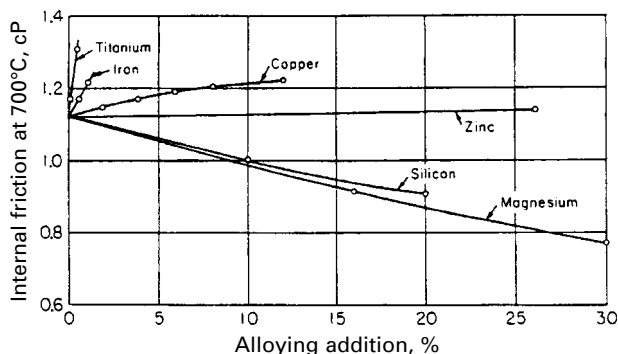
favour nucleation of hydrogen bubbles. Homogeneous nucleation of hydrogen bubbles in liquid aluminium is impractical. Therefore heterogeneous nucleation in the presence of imperfections or minute inclusions in the metal is the primary mechanism of bubble formation. The growth of pores after nucleation is a diffusion controlled process. The probability of hydrogen bubble entrapment during laser beam welding is governed by the viscosity and cooling rate of the molten weld pool. According to Stokes law, the rising speed u of a spherical gas bubble in a viscous liquid is given by

$$u = \frac{2r^2 \Delta \rho g}{9\mu} \quad \dots \quad (19)$$

where r is the radius of the bubble, $\Delta \rho$ is the density difference between the liquid and the gas bubble, and μ is the viscosity of the liquid. The chances of porosity formation by entrapment of a hydrogen bubble in the weld pool are increased by high liquid viscosity and small bubble radius.

The cooling rate of the molten weld pool controls the growth and escape of any hydrogen bubbles which nucleate. At high cooling rates, the time available for bubble growth and escape is reduced. Therefore, high cooling rates lead to the formation of small pores. For castings of Al-4.7 Mg alloys, Fang *et al.*¹⁰⁷ have shown that the average size of hydrogen porosity decreases with increasing cooling rates. Higher cooling rates give less time for hydrogen to diffuse, causing reduction in pore volume,¹⁰⁷ as shown in Fig. 23. Many other investigations¹⁰⁸⁻¹¹⁰ have shown that the volume fraction of hydrogen porosity is reduced as the cooling rate increases. In the case of laser beam welding, the cooling rates are much faster than in casting and a much smaller hydrogen pore size is to be expected.

The effect of alloying elements on hydrogen porosity formation is not well understood. These effects can be considered by examining the way in which the alloying additions affect the hydrogen



24 Effect of addition of alloying elements on viscosity of aluminium³³

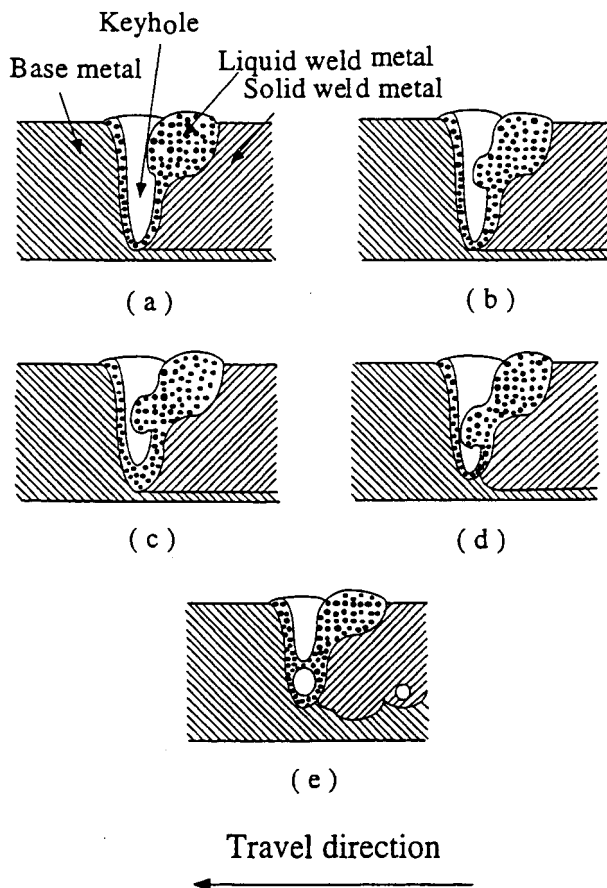
solubility in aluminium, the viscosity of molten aluminium, and the interfacial energy by acting as surfactants. An alteration in hydrogen solubility in the presence of alloying elements affects the threshold hydrogen concentration for porosity formation. The effect of alloying elements on the viscosity of molten aluminium is shown³³ in Fig. 24. Surface active elements such as lithium, magnesium, bismuth, and lead can reduce the interfacial energy and aid the nucleation of hydrogen bubbles. The overall effect of alloying elements on the tendency for hydrogen porosity formation may depend on a combination of all three factors. However, because of the high cooling rate associated with laser beam welding, the presence of hydrogen may lead to micropores. The macropores cannot be attributed to hydrogen solubility.

In conventional welding processes, the primary sources of hydrogen in the weld metal are the filler metal, the shielding gas, and the base metal. Eliminating hydrogen from these sources can effectively control porosity formation. However, in laser welding this is not achieved. Marsico⁵ reported that severe porosity in the weld metal was consistently observed during autogenous laser welding of aluminium alloys, even when hydrogen was eliminated from all possible sources, indicating that the main source of macroporosity may not be hydrogen. An alternative mechanism has to be considered as the cause of macroporosity formation in laser beam welding.

Porosity due to collapse of keyhole

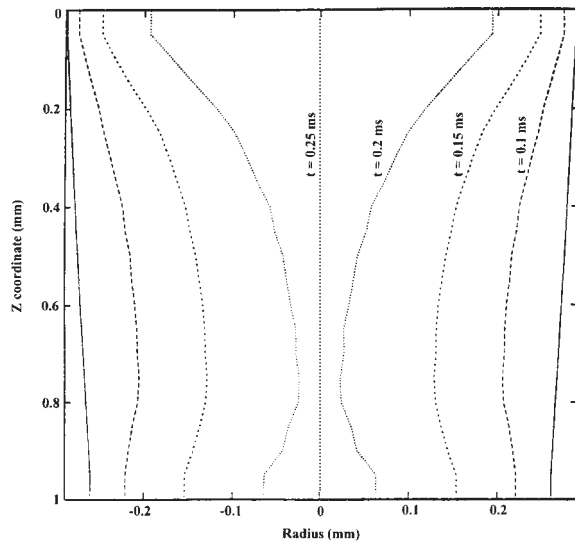
The entrapment of gaseous species, including vapourised alloying elements and the shielding gas, due to the instability and collapse of the keyhole can be considered as a possible cause of porosity in laser welding of aluminium alloys. During keyhole mode welding, as the keyhole moves forward, the liquid metal on the rear wall moves in to fill the space vacated by the front wall of the keyhole. If the keyhole wall is unstable, the metal may fail to fill the cavity smoothly behind the fast moving laser beam, as shown schematically in Fig. 25.¹¹¹ As a result, the metal vapours and gases are entrapped at the root of the weld. Therefore, establishing a stable keyhole is very important for obtaining a good quality weld.

The collapse of a moving keyhole has yet to be formulated theoretically, although the behaviour of a stationary keyhole has been modelled.¹¹²⁻¹¹⁵ In early



25 Schematic diagram showing formation of void at weld root due to imperfect collapse of keyhole¹¹¹

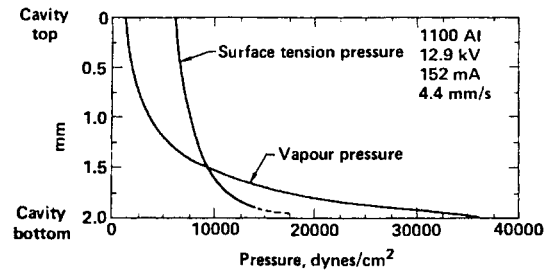
studies, Rayleigh¹¹² and Bachelor¹¹³ established a theoretical foundation for the collapse of a spherical bubble. Later, Kroos *et al.*¹¹⁴ formulated the problem in a cylindrical geometry to simulate the collapse of a keyhole in laser welding. The pressure on the keyhole wall was considered mainly to be a result of the balance between the ablation pressures and the surface tension forces. The dynamic pressure due to fluid flow and the hydrostatic pressure were considered to be negligible. Their predicted keyhole radius was ≥ 1.7 times the laser beam radius. They also calculated the collapse time of the cylindrical keyhole following sudden laser beam shutdown. The typical calculated closing time of the keyhole for aluminium, iron, and copper was of the order of 0.1 ms. This result implies that if the interval between two successive pulses during pulsed laser welding exceeds 0.1 ms, the resulting weld will not be continuous. More recently, Ducharme *et al.*¹¹⁵ included the axial variation of the keyhole geometry in their calculations. They calculated the collapse time of a keyhole following the extinction of a CO₂ laser beam during laser welding of iron and aluminium. The initial radius of the keyhole was first calculated using an integrated keyhole and weld pool model.¹¹⁶ It was assumed that the pressure in the keyhole drops to the ambient atmospheric pressure in a period much shorter than the time necessary for the collapse of the keyhole. The keyhole was considered to collapse because of



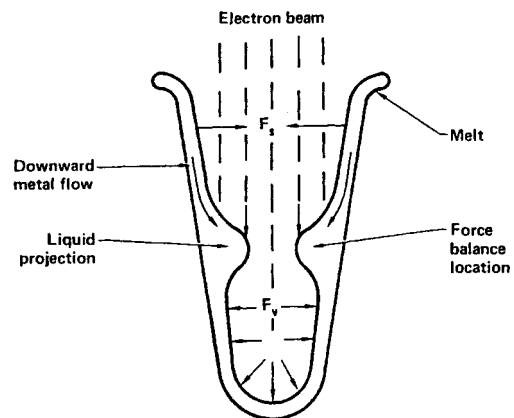
26 Keyhole wall profiles during CO₂ laser welding of 1.0 mm thick aluminium sheet at time t following extinction of laser beam:¹¹⁵ laser power 2 kW, welding speed 10 mm s⁻¹

the surface tension forces acting on the keyhole wall. The calculations involved the equation of continuity and Navier–Stokes equations. The keyhole wall was treated as a moving boundary. The keyhole geometry in aluminium sheet at various collapse times is shown in Fig. 26. It is interesting to note that the keyhole collapses faster in the middle of the keyhole wall, which may result in entrapment of gas bubbles at the bottom of the keyhole. Matsunawa *et al.*¹¹⁷ found this type of porosity near the bottom of the fusion zone in pulsed laser welding of aluminium alloys. They showed that such porosity could be prevented by improving the shape of the laser pulse.

Schauer and Giedt¹¹⁸ studied keyhole stability in electron beam welding. The problem is pertinent to laser welding because the conditions for containing a stable keyhole are the same in these two processes. Forces on the keyhole wall were considered mainly to be a result of the balance between the vapour pressure and the surface tension force. Based on the measured temperature profile as a function of position on the keyhole wall, they calculated the vapour pressure force and the surface tension profile along the keyhole wall. The typical calculated profiles of surface tension pressure and vapour pressure along the keyhole depth during electron beam welding of 1100 aluminium are shown in Fig. 27. It is observed from this figure that the surface tension force is greater than the vapour pressure force in the upper region of the keyhole, and lower in the lower region. A projection is likely to form in the upper region of the keyhole due to the high surface tension force, as shown in Fig. 28. The liquid in this projection will have been preheated when it moves to the bottom of the keyhole. The electron beam can easily bore through this superheated liquid causing a sudden increase in keyhole depth. The process may happen periodically, resulting in spiking.¹¹⁸ Voids tend to form in the lower portions of the spikes because molten metal does not fill the region completely as the keyhole collapses.¹¹⁸



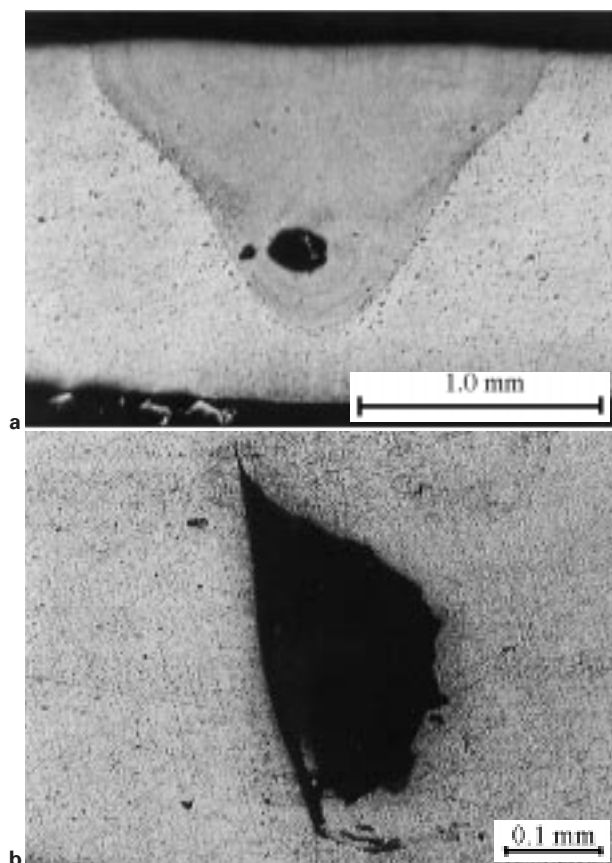
27 Calculated values for surface tension pressure and vapour pressure in 1100 aluminium electron beam welding cavity as function of cavity depth¹¹⁸



28 Liquid projection formation at location where surface tension force is nearly in balance with vapour pressure force¹¹⁸

Schauer and Giedt¹¹⁸ found that the tendency to spike formation could be evaluated by a stability parameter $S = H/h$, where H is the height between the keyhole bottom and where the liquid projection forms and h is the penetration depth of the keyhole. Based on their experimental data, they proposed that spiking would not be a problem for welds with $S < 0.5$. However, when S was > 0.5 , the weld might be expected to exhibit unacceptable spiking. The narrow, deep shaped keyhole geometry tends to have higher value of S ; therefore, spiking is frequently found during deep penetration keyhole mode welding. On the other hand, the surface tension and the equilibrium vapour pressure of the welded material are two important parameters in determining the stability of the keyhole.

Many automotive aluminium alloys have lower surface tensions than 1100 due to the presence of surface active elements such as magnesium. At the same time, they have higher vapour pressures due to the presence of volatile elements such as magnesium, manganese, and zinc. Therefore, the surface tension pressure curve in Fig. 27 will be lower and the vapour pressure curve in the figure will be higher for welding of automotive aluminium alloys. As a result, the stability parameter S is high for the welding of these alloys if the penetration depth h and other conditions are the same. Therefore, laser welding of automotive aluminium alloys tends to have poor keyhole stability and is more susceptible to formation of porosity due to the instability of the keyhole.



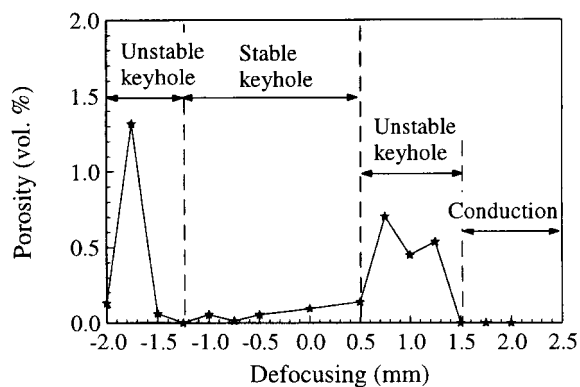
a spherical porosity near bottom of weld pool; b irregularly shaped porosity at fusion line

29 Typical porosity observed during Nd-YAG laser welding of 5754 aluminium alloy²⁴

Recent investigations^{24,66,111} on pore formation during continuous wave Nd-YAG laser welding of 5182 and 5754 aluminium alloys have confirmed the importance of keyhole stability in the formation of porosity. Macropores 0.2 mm or larger in size dominated the porosity distribution, as shown in Fig. 29. The amount of macroporosity produced at several beam defocus values during laser welding of 5754 alloy is presented in Fig. 30. The data show that when the welding was conducted in the transition region between the keyhole and the conduction modes, macroporosity was consistently observed. Since hydrogen is generally considered to be the main cause of porosity in aluminium alloys, the role of hydrogen in pore generation was examined by using both wet and dry helium as the shielding gas during laser welding. It was found that the presence of moisture in the shielding gas did not increase the amount of macroporosity in the weld, although small amounts of microporosity were observed in some rare cases.¹¹¹ These studies^{24,66,111} also showed that when welding parameters were properly chosen to avoid the transition region where the keyhole is unstable, porosity could be minimised.

Hot cracking

The restrained contraction of a weld during cooling sets up tensile stresses in the joint and may cause cracking, one of the most serious weld defects. There



30 Porosity produced at several beam defocusing values during Nd-YAG laser welding of 5754 aluminium alloy:¹¹¹ laser power 3.0 kW, welding speed 150 in min⁻¹, shielding gas pure helium at flowrate of 200 ft³ h⁻¹

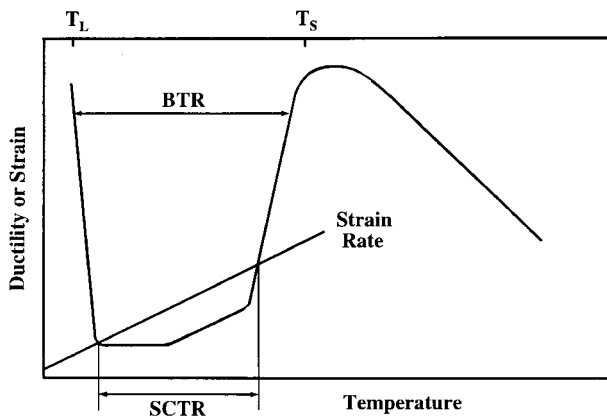
are two kinds of hot cracking: cracking that occurs in the weld fusion zone during solidification of the weld metal is known as solidification cracking, whereas cracking that takes place in the partially melted zone due to liquation of low melting point components is known as liquation cracking. Aluminium alloys may be susceptible to both solidification cracking and liquation cracking during fusion welding. In laser welding of aluminium alloys, solidification cracking has been reported,^{79,117,119-121} while liquation cracking has rarely been observed⁷³ due to the low heat input and small heat affected zone of the laser welds. Therefore, the following discussion focuses on the mechanism of solidification cracking, susceptibility of various alloys to cracking, and the available remedies.

Mechanism of solidification cracking

Certain special features are commonly observed when solidification cracking occurs:

- (i) the fractured surface is always dendritic in nature
- (ii) fracture usually occurs at the grain boundaries
- (iii) the crack tip is dull
- (iv) the fractured surface is usually covered with oxides if the crack reaches the specimen surface where it can be exposed to oxygen, otherwise it has a silvery colour characteristic of unoxidised metal.

Most alloys pass through a brittle temperature range (BTR) during solidification, as shown in Fig. 31.¹²² Weld solidification cracking susceptibility is related to the extent of the BTR of the alloy. Solidification cracking occurs when the thermal tensile strains induced by internal contraction and external displacement exceed the ductility of the weld metal within the BTR. Many theories have been proposed regarding the mechanism of solidification cracking.¹²³⁻¹²⁷ Automotive aluminium alloys such as 2xxx (Al-Cu), 5xxx (Al-Mg), and 6xxx (Al-Mg₂Si) usually form low melting point eutectics during solidification. Solidification cracking of these alloys is mainly associated with the alloying elements rather than, as in the case of steel, with the presence of low melting



31 Weld metal ductility during and following solidification.¹²² BTR and SCTR represent brittle and solidification cracking temperature range respectively

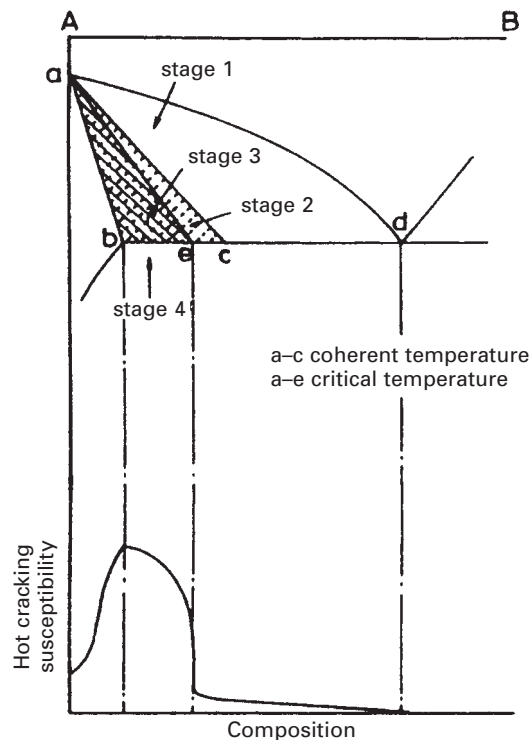
point impurities. The generalised theory proposed by Borland¹²⁷ explained the solidification behaviour and the crack susceptibility of alloys that form low melting eutectics. The solidification process was divided into four stages, as shown in Fig. 32, with the corresponding cracking susceptibility curve:

- (i) stage 1: as a liquid alloy is cooled below its liquidus temperature, solid crystals nucleate and grow until, at a certain temperature (the coherent temperature), they join together to form a coherent mass; although not completely solidified, the alloy first acquires mechanical strength at this temperature; no cracking occurs due to the presence of a large quantity of residual liquid
- (ii) stage 2: interlocking of dendrites starts: residual liquid is still capable of moving between the interlocking dendrites to refill and heal any initiated crack; therefore, no crack is formed at this stage
- (iii) stage 3: the 'critical solidification' range: residual liquid is discontinuous due to the presence of a semicontinuous network of solid; no refilling or healing is possible once cracks are initiated as a result of thermal strains
- (iv) stage 4: the alloy is completely solidified: no cracks develop at this stage due to the high strength of the solid.

Matsuda *et al.*¹²⁸ reported that the temperature ranges in the above stages 1 and 2 were much narrower during welding than other slow cooling processes. Furthermore, stage 3 could be subdivided into two stages, 3(h) at higher temperature and 3(l) at lower temperature. Almost all the cracks were initiated at stage 3(h) because the residual liquid between grain boundaries was in the form of a continuous film. During stage 3(l) the joint was susceptible to crack propagation but not to crack initiation because the residual liquid was in the form of droplets.

Solidification cracking susceptibility

According to the generalised theory,¹²⁷ the magnitude of the critical solidification range is proportional to the difference between the nominal liquidus and solidus temperatures. An alloy has the highest solidifi-

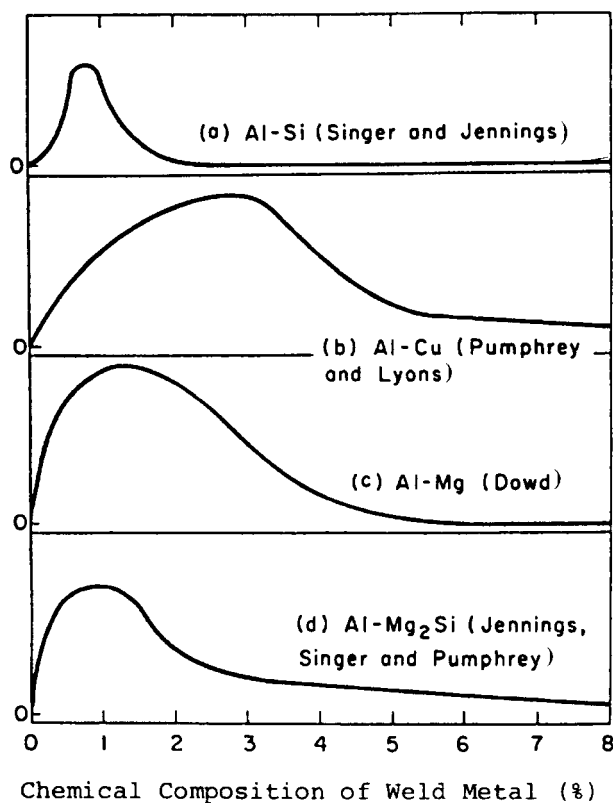


32 Effect of constitutional features on cracking susceptibility in binary systems¹²⁷

cation crack susceptibility if its critical temperature range is the widest, i.e. composition b in Fig. 32. However, due to the highly non-equilibrium solidification during laser welding, the actual solidus temperature of the alloy is depressed, resulting in a wider critical solidification temperature range and, therefore, higher solidification crack susceptibility. Moreover, the composition which has the highest solidification crack susceptibility is shifted from b in Fig. 32 to a more solvent rich composition.¹²⁹ The effect of chemical composition of weld metal on crack susceptibility in various aluminium binary alloys is given¹²⁹ in Fig. 33. It is observed that aluminium alloys have the highest solidification crack susceptibility when the compositions are 0.6%Si in Al-Si alloys, 1-3%Cu in Al-Cu alloys, 1-1.5%Mg in Al-Mg alloys, and 1.0%Mg₂Si in Al-Mg-Si alloys.

The solidification cracking susceptibility of aluminium alloys is also process sensitive. It was recently reported^{79,119-121} that pulsed laser welding of aluminium alloys is characterised by much higher solidification crack susceptibility than continuous laser welding. Patterson and Milewski¹³⁰ reported a similar observation comparing pulsed and continuous gas tungsten arc welding of alloy 625 to 304L stainless steel. These observations are contrary to the early views^{131,132} that pulsed current welding may decrease weld cracking susceptibility due to the reduced heat input and compositional segregation.

Increased crack susceptibility during pulsed welding can be attributed to the increased cooling rate which causes a high thermal strain rate,^{79,80,117} increased stress gradient,¹³⁰ and lack of refilling of the developing cracks.¹²¹ It is likely that crack initiation by strain evolution competes with crack healing through refilling by the residual liquid. While



33 Effect of chemical composition of weld metal on relative crack susceptibility (ordinate) in various aluminium binary alloys¹²⁹

the crack initiation rate increases with thermal strains, the refilling and healing movement of the residual liquid is controlled by its fluidity. High cooling rates cause rapidly developing thermal shrinkage strains that result in a high crack initiation rate. Meanwhile, high cooling rates also reduce the time available for the residual liquid to refill and heal the initiated cracks. Therefore, a higher cooling rate is responsible for the increased solidification crack susceptibility in pulsed laser welding of aluminium alloys.

Prevention of solidification cracking

The occurrence of solidification cracking in laser welding of aluminium alloys is closely related to the chemical composition and microstructure of the alloys and the magnitude and rate of thermal strains during welding. Therefore, the following measures can be taken to prevent solidification cracking.

Improve welding materials

The composition of the weld metal should be controlled to avoid the high solidification cracking susceptibility ranges shown in Fig. 33. Type 5xxx alloys used in the automotive industry are usually not susceptible to solidification cracking due to their high magnesium concentrations: 2xxx and 6xxx alloys, on the other hand, have higher solidification crack susceptibility.^{86–88} Therefore, in case of continuous laser welding, the 5xxx alloys can be welded autogenously without solidification cracking, while 2xxx and 6xxx alloys require use of filler metals such as 4043 and 4047 to modify the composition and avoid solidifi-

cation cracking. For example, a low crack susceptibility is achieved when silicon contents in 6xxx alloys are 2% or more.^{78,133–135}

Refine solidification structure

The solidification structure of the weld metal can be modified to increase solidification crack resistance. Trace elements such as titanium and zirconium can significantly refine the solidification structure of the aluminium weld metal.¹³⁶ Therefore, small additions of these elements can improve the solidification cracking resistance of aluminium alloys. Other grain refining techniques such as magnetic stirring,¹³⁷ beam oscillation,¹³⁸ and surface cooling¹³⁹ can also be used if necessary.

Optimise pulsed laser welding

Pulsed laser welding has the beneficial effect of producing grain refinement. It also offers higher process control flexibility. However, pulsing of the laser power increases the likelihood of solidification cracking due to the high cooling rates and rapid solidification.^{79,80} Therefore, optimisation of pulsing is required to avoid hot cracking. It has been shown that proper pulse shape and sequence of the laser beam can reduce strain rate and promote crack refilling.^{53,121}

Reduce thermal strains

Thermal strains in welding are influenced by the welding process, heat input, joint configuration and rigidity, and the thermal properties of the welded metals. Thermal tensile strains or displacement can be minimised by designing proper welding fixture and joint configuration, controlling weld bead shape to obtain a lower aspect ratio (H/W), and maintaining an elliptical puddle instead of a teardrop shaped puddle¹⁴⁰ by using high heat input and low welding speed.¹⁴¹

Important unanswered questions

Although laser beam welding is widely used in the industry, several scientific and technological problems have not been satisfactorily solved. A selection of these important problems is presented below.

Control of alloying elements loss

The loss of volatile alloying elements by vaporisation during laser welding of automotive aluminium alloys is a severe problem which causes degradation of the mechanical properties of the welds. It is known that the rate of vaporisation in laser welding is determined by many factors such as temperature distribution on the weld pool surface, local concentrations of the alloying elements, and possibly by other factors. Control of beam power density distribution during continuous wave mode laser welding and adjustments of pulsing parameters during pulsed beam welding can reduce the surface temperature. The lower temperature, in turn, may alleviate, at least in part, the alloying element loss. In non-autogenous welding, the composition of the filler metal may be carefully chosen to compensate for the loss of alloying elements. However, no unified, science based procedure currently exists to entirely avoid the loss of alloying elements during laser welding of automotive aluminium alloys.

Table 2 Thermophysical properties of aluminium and iron*: all data from Ref. 143 unless indicated; α and Pr are derived quantities

	ρ , kg m ⁻³	k , W m ⁻¹ K ⁻¹	c_p , J kg ⁻¹ K ⁻¹	α , m ² s ⁻¹	μ , kg m ⁻¹ s ⁻¹	Pr	σ , N m ⁻¹	$d\sigma/dT$, N m ⁻¹ K ⁻¹
Al at melting point (933 K)	2385	94.03	1080	3.65×10^{-5}	0.0013	0.015	0.914	-3.5×10^{-4}
Al at 673 K	2620	238	1076	8.44×10^{-5}
Fe at melting point (1810 K)	7015	38†	795	6.80×10^{-6}	0.0055	0.12	1.872	-4.9×10^{-4}
Fe at 673 K	7747	48.6	611	1.03×10^{-5}

* ρ , k , c_p , α , μ , Pr , σ , and $d\sigma/dT$ represent density, thermal conductivity, specific heat, thermal diffusivity, viscosity, Prandtl number, surface tension, and temperature coefficient of surface tension respectively.

† From Ref. 144.

Control of porosity formation

Avoiding porosity formation remains an important goal in laser welding of automotive aluminium alloys. It is known that the dissolution and release of hydrogen from the weld pool is the primary cause of microporosity. Furthermore, macroporosity is caused by the imperfect collapse of the keyhole. A comprehensive study of these two types of porosity in automotive aluminium alloys has not been carried out. A better understanding of the dynamics and stability of the keyhole will serve as a basis to prevent the formation of macroporosity.

Control of weld pool geometry

Achieving reproducible, defect free, full penetration welds is an important goal of laser welding of automotive aluminium alloys. Acceptable combinations of welding variables are currently obtained by trial and error. However, in many cases, adjustment of welding variables by conducting a large number of experiments is time consuming and expensive. Development of numerical models based on comprehensive phenomenological understanding of the process and material has provided an effective way to calculate the weld pool geometry. Such efforts to understand the laser welding of automotive aluminium alloys are just beginning.

Better understanding of role of surface active elements

Surface active elements in aluminium alloys such as bismuth, lead, antimony, calcium, and tin can potentially affect the laser welding of aluminium alloys in several ways. First, they may significantly influence the fluid flow pattern and the keyhole stability by changing the surface tension of the molten metal. Second, they may affect the vaporisation rates of the alloying elements by two opposing effects: inhibiting vaporisation by covering a part of the available vaporising surface; and enhancing vaporisation by causing interface turbulence which increases the surface area. Third, the surface active elements reduce the interfacial energy and aid in the nucleation of hydrogen pores. It is not clear if the surface active elements can be utilised to achieve improved weld penetration, lower vaporisation rates of alloying elements, and minimise porosity formation.

Mechanical behaviour and formability

The heat affected zone, loss of alloying elements, the presence of defects such as cracks and porosity, as

well as weld bead geometry (e.g. undercut, root sag, etc.) all affect the mechanical behaviour and formability of laser welded aluminium alloy joints. An improved understanding of the mechanical properties of joints as a whole and the ability to control mechanical properties are much needed. Better formability data and research on formability improvement are also critical to wider use of laser welded aluminium, as the adoption of aluminium laser welded tailored blanks and, in the future, hydroformed aluminium structures depends particularly on the availability of this information.

Process robustness

Research to date has indicated that laser welding of aluminium is not a particularly robust process. Small variations in processing parameters often have a major impact on joint properties.¹⁴² For widespread use in the automotive industry, larger process variable windows are needed. Research on increasing the predictability and robustness of the process in the presence of the disturbances which commonly occur in a manufacturing environment is more important to the broader use of this technology than optimising the process in a very narrow operating region. This topic has not been adequately addressed to date for the welding of automotive aluminium alloys.

Outlook

In recent years, significant progress has been made in understanding the laser welding of automotive aluminium alloys. In particular, investigations at the crossroads of basic and applied sciences have led to new insights into the physical processes in welding as well as the geometry, composition, structure, and properties of the welded alloys. However, several key problems and issues remain to be addressed. These issues have major design and manufacturing significance, and their investigation is particularly timely as government and industry jointly push for expanded use of lightweight materials in automobile bodies.

Making the most weight and cost effective use of aluminium in automobile bodies will require use of tailor welded blanks. Laser welding is the preferred fabrication method. However, to date, laser welding of aluminium has been poorly understood. As the lasers get less expensive and more reliable, their applications in the automotive industry are expected to grow. Enhanced use of laser welded aluminium alloy tailor welded blanks and other automotive components will be driven both by the internal need for cost competitiveness and quality improvements

and by the external push to comply with the increasingly stringent environmental and energy related regulations.

Acknowledgement

Financial support for this work was provided by the US Department of Energy (grant DE-FG02-96ER45602). The authors thank Professor K. P. Abraham and Dr S. A. David for their interest in this work.

References

- E. HAGEN and H. RUBENS: *Annl. Phys.*, 1902, **4**, (8), 1–21.
- M. A. BRAMSON: 'Infrared radiation: a handbook for applications'; 1968, New York, Plenum Press.
- W. W. DULEY: 'Laser processing and analysis of materials', 71; 1983, New York, Plenum Press.
- C. A. HUNTINGTON and T. W. EAGAR: *Weld. J.*, 1982, **62**, (4), 105s.
- T. MARSICO: MS thesis, The Pennsylvania State University, PA, USA, 1988.
- Y. ARATA and I. MIYAMOTO: *Technocrat*, May 1978, **11**, (5), 33.
- K. BEHLER, E. BEYER, and R. SCHAFER: Proc. ICALEO '88: 'Laser materials processing', 249; 1988, Orlando, FL, Laser Institute of America.
- R. C. CRATER: Proc. 4th Int. Conf. on 'Advances in welding processes', 267; 1978, Cambridge, The Welding Institute.
- 'Welding Kaiser aluminium', 2nd edn; 1978, Oakland, CA, Kaiser Aluminium Co.
- R. JAN, P. R. HOWELL, and R. P. MARTUKANITZ: '4th international conference on trends in welding research', (ed. H. B. Smartt *et al.*), 329; 1996, Materials Park, OH, ASM International.
- H. SAKAMOTO, K. SHIBATA, and F. DAUSINGER: Proc. ICALEO '92: 'Laser materials processing', (ed. D. Farson *et al.*), 523; 1992, Orlando, FL, Laser Institute of America.
- S. KATAYAMA: *J. Light Met. Weld. Constr.*, 1996, **34**, (4), 23.
- P. W. FUERSCHBACH: *Weld. J.*, 1996, **75**, (1), 24s.
- T. DEBROY and S. A. DAVID: *Rev. Mod. Phys.*, 1995, **67**, (1), 85.
- A. MATSUNAWA, H. YOSHIDA, and S. KATAYAMA: Proc. ICALEO '84, Vol. 44, 35–42; 1984, Orlando, FL, Laser Institute of America.
- C. M. BANAS: 'The industrial laser annual handbook', 69–86; 1986, Tulsa, OK, PennWell Books.
- D. R. KEEFER: 'Laser-induced plasmas and applications', (ed. L. J. Radziemski and D. A. Cremers), 169–206; 1989, New York, Marcel Dekker.
- T. D. ROCKSTROH and J. MAZUMDER: *J. Appl. Phys.*, 1987, **61**, (3), 917.
- R. MILLER and T. DEBROY: *J. Appl. Phys.*, 1990, **68**, (5), 2045.
- D. A. SCHAUER, W. H. GIEDT, and S. M. SHINTAKU: *Weld. J.*, 1978, **57**, (5), 127s–133s.
- C. R. HEIPLE and J. R. ROPER: in 'Trends in welding research in the United States', (ed. S. A. David), 489–520; 1982, Metals Park, OH, ASM.
- H. G. KRAUS: *Weld. J.*, 1989, **68**, 269s.
- S. KOU and Y. H. WANG: *Metall. Trans. A*, 1986, **17A**, 2265–2270.
- M. PASTOR, H. ZHAO, R. P. MARTUKANITZ, and T. DEBROY: *Weld. J.*, 1999, **78**, (6), 207s–216s.
- S. KOU and Y. H. WANG: *Weld. J.*, 1986, **65**, (3), 63s–70s.
- T. ZACHARIA, A. H. ERASLAN, and D. K. AIDUN: *Weld. J.*, 1988, **67**, 53s–62s.
- K. HONG: PhD thesis, University of Waterloo, Waterloo, Ont., Canada, 1996.
- S. KOU and Y. LE: *Metall. Trans. A*, 1983, **14A**, 2245–2253.
- W. PITSCHENEDER, T. DEBROY, K. MUNDRA, and R. EBNER: *Weld. J.*, 1996, **75**, (3), 71s.
- P. SAHOO, T. DEBROY, and M. J. McNALLAN: *Metall. Trans. B*, 1988, **19B**, 483.
- P. R. SCHELLER, R. F. BROOKS, and K. C. MILLS: *Weld. J.*, 1995, **74**, (2), 69s.
- L. GUMIRI *et al.*: *Surf. Sci.*, 1979, **83**, 471.
- J. E. HATCH: 'Aluminium: properties and physical metallurgy'; 1984, Metals Park, OH, ASM.
- J. GOICOECHEA, C. GARCIA-CORDOVILLA, E. LOUIS, and A. PAMIES: *J. Mater. Sci.*, 1992, **27**, (19), 5247.
- D. E. SWIFT-HOOK and A. E. F. GICK: *Weld. J.*, 1973, **52**, (11), 492s–499s.
- J. G. ANDREWS and D. R. ATTHEY: *J. Phys. D: Appl. Phys.*, 1976, **9**, 2181.
- P. G. KLEMENS: *J. Appl. Phys.*, 1976, **47**, (5), 2165.
- J. MAZUMDER and W. M. STEEN: *J. Appl. Phys.*, 1980, **51**, (2), 941.
- J. DOWDEN, M. DAVIS, and P. KAPADIA: *J. Fluid Mech.*, 1983, **126**, 123.
- M. DAVIS, P. KAPADIA, and J. DOWDEN: *Weld. J.*, 1986, **65**, (7), 167s–174s.
- J. DOWDEN, N. POSTACIOGLU, M. DAVIS, and P. KAPADIA: *J. Phys. D: Appl. Phys.*, 1987, **20**, 36.
- N. POSTACIOGLU, P. KAPADIA, M. DAVIS, and J. DOWDEN: *J. Phys. D: Appl. Phys.*, 1987, **20**, 340.
- A. KAR and J. MAZUMDER: *J. Appl. Phys.*, 1995, **78**, (11), 6353.
- P. S. MOHANTY and J. MAZUMDER: *Sci. Technol. Weld. Join.*, 1997, **2**, (3), 133.
- W. M. STEEN, J. DOWDEN, M. DAVIS, and P. KAPADIA: *J. Phys. D: Appl. Phys.*, 1988, **21**, 1255.
- G. HERZIGER *et al.*: in 'Laser materials processing', 55; 1984, New York, Plenum Press.
- A. KAR, T. ROCKSTROH, and J. MAZUMDER: *J. Appl. Phys.*, 1992, **71**, 2560.
- M. BECK, P. BERGER, and H. HUGEL: Proc. ECLAT '92: 'Laser treatment of materials', (ed. B. L. Mordike), 693–698; 1992, Oberursel, DGM Informationsgesellschaft.
- A. KAPLAN: *J. Phys. D: Appl. Phys.*, 1994, **27**, 1805.
- J. KROOS, U. GRATZKE, and G. SIMON: *J. Phys. D: Appl. Phys.*, 1993, **26**, 474.
- E. A. METZBOWER: *Metall. Trans. B*, 1993, **24B**, 875.
- A. CYBULSKI and Z. MUCHA: *Weld. Int.*, 1997, **11**, (3), 212.
- A. MATSUNAWA, J. D. KIM, N. SETO, M. MIZUTANI, and S. KATAYAMA: *J. Laser Appl.*, 1998, **10**, (6), 247.
- J. KROOS, U. GRATZKE, M. VICANEK, and G. SIMON: *J. Phys. D: Appl. Phys.*, 1993, **26**, 481.
- T. KLEIN, M. VICANEK, J. KROOS, I. DECKER, and G. SIMON: *J. Phys. D: Appl. Phys.*, 1994, **27**, 2023.
- A. MATSUNAWA and V. SEMAK: *J. Phys. D: Appl. Phys.*, 1997, **30**, 798.
- I. MIYAMOTO and H. MARUO: *Weld. Int.*, 1996, **10**, (6), 448.
- P. A. A. KHAN, T. DEBROY, and S. A. DAVID: *Weld. J.*, 1988, **67**, (1), 1s–7s.
- L. R. MORRIS *et al.*: in 'Aluminium transformation technology and applications', (ed. C. A. Pampillo *et al.*), 549–582; 1982, Metals Park, OH, ASM.
- D. W. MOON and E. A. METZBOWER: *Weld. J.*, 1983, **62**, (2), 53s–58s.
- T. LIDA and R. I. L. GUTHRIE: 'The physical properties of liquid metals', 88; 1993, Oxford, Clarendon Press.
- A. BLOCK-BOLTEN and T. W. EAGAR: *Metall. Trans. B*, 1984, **15B**, 461.
- M. M. COLLUR, A. PAUL, and T. DEBROY: *Metall. Trans. B*, 1987, **18B**, 733.
- P. SAHOO, M. M. COLLUR, and T. DEBROY: *Metall. Trans. B*, 1988, **19B**, 967.
- F. D. RICHARDSON: 'Physical chemistry of melts in metallurgy', Vol. 2, 452–453; 1974, London, Academic Press.
- M. PASTOR, H. ZHAO, and T. DEBROY: Proc. Natl. Welding Seminar '97, 31–46; 1997, Calcutta, Indian Institute of Welding.
- T. DEBROY, S. BASU, and K. MUNDRA: *J. Appl. Phys.*, 1991, **70**, 1313.
- K. MUNDRA and T. DEBROY: *Metall. Trans. B*, 1993, **24B**, 145.
- K. MUNDRA and T. DEBROY: *Weld. J.*, 1993, **72**, (1), 1s.
- C. L. CHAN and J. MAZUMDER: *J. Appl. Phys.*, 1987, **62**, 4579.
- H. ZHAO and T. DEBROY: 'Modeling of composition change during laser welding of aluminium alloys', Internal Report, Department of Materials Science and Engineering, The Pennsylvania State University, PA, USA, 1998.
- L. A. GUITERREZ, G. NEYE, and E. ZSCHECH: *Weld. J.*, 1996, **75**, (4), 115s–121s.
- S. KATAYAMA, C. D. LUNDIN, and J. C. DANKO: 'Recent trends in welding science and technology', (ed. S. A. David and J. M. Vitek), 687–691; 1990, Materials Park, OH, ASM International.
- I. JONES, S. RICHES, J. W. YOON, and E. R. WALLACH: Proc. LAMP '92, Nagaoka, Japan, June 1992, High Temperature Society of Japan, 523–528.
- C. RAMASAMY and C. E. ALBRIGHT: 'CO₂ and Nd-YAG laser beam welding of aluminium alloy 6111-T4', Edison Welding Institute, Columbus, OH, USA, 1998.

76. C. RAMASAMY and C. E. ALBRIGHT: 'CO₂ and Nd-YAG laser beam welding of aluminium alloy 5754-O', Edison Welding Institute, Columbus, OH, USA, 1998.
77. S. VENKAT, C. E. ALBRIGHT, S. RAMASAMY, and J. P. HURLEY: *Weld. J.*, 1997, **76**, (7), 275s-282s.
78. M. KUTSUNA, J. SUZUKI, S. KIMURA, S. SUGIYAMA, M. YUHKI, and H. YAMAOKA: *Weld. World*, 1993, **31**, (2), 126-135.
79. M. J. CIESLAK and P. W. FUERSCHBACH: *Metall. Trans. B*, 1988, **19B**, 319.
80. S. KRISHNASWAMY and W. BAESLACK: *Mater. Charact.*, 1990, **24**, 331-353.
81. J. MAZUMDER and S. BHANDARI: 'Laser welding of aluminium alloys', Report to Ford Motor Co., Dearborn, MI, USA, July 1999.
82. T. STARZER, R. EBNER, W. GLATZ, F. ELLERMANN, and W. KUEHL-EIN: Proc. 26th Int. Symp. on 'Automotive technology and automation': 'Laser applications in the automotive industries', Aachen, Germany, September 1993, 131-138.
83. R. P. MARTUKANITZ, F. G. ARMAO, B. ALTSHULLER, and E. R. PICKERING: SAE 1996 Int. Cong. and Exposition Reprint, SAE International, Warrendale, PA, USA, 1996.
84. R. P. MARTUKANITZ and D. J. SMITH: Proc. 6th Int. Conf. on 'Aluminium weldments', 309; 1995, Miami, FL, AWS.
85. D. J. SMITH: MS thesis, The Pennsylvania State University, PA, USA, 1994.
86. R. P. MARTUKANITZ and B. ALTSHULLER: Proc. ICALEO '96: 'Lasers and electro-optics for automotive manufacturing', Vol. 82, 39; 1996, Orlando, FL, Laser Institute of America.
87. P. A. HILTON: *Opt. Quantum Electronics*, 1995, **27**, 1127-1147.
88. J. RAPP, C. GLUMANN, F. DAUSINGER, and H. HUGEL: *Opt. Quantum Electronics*, 1995, **27**, 1203-1211.
89. R. F. ASHTON and R. P. WESLEY: *Weld. J.*, 1975, **54**, (3), 95s.
90. M. KATO: *J. Light Met. Weld. Constr.*, 1996, **34**, (4), 42.
91. K. P. ABRAHAM and T. DEBROY: *Alum. India*, 1998, **15**, (2), 13-18.
92. T. B. MASSALSKI: 'Binary alloy phase diagrams', Vol. 1; 1990, Materials Park, OH, ASM International.
93. E. T. TURKDOGAN: 'Physical chemistry of high temperature technology', 5; 1980, New York, Academic Press.
94. J. F. ELLIOTT and M. GLEISER: 'Thermochemistry for steelmaking (I)', 75; 1963, Reading, MA, Addison-Wesley.
95. S. KATAYAMA: *J. Light Met. Weld. Constr.*, 1996, **34**, (4), 199.
96. C. E. RANSLEY and H. NEUFELD: *J. Inst. Met.*, 1947-48, **74**, 599.
97. W. R. OPIE and N. J. GRANT: *J. Met.*, 1950, **188**, 1237.
98. W. BAUKLOH and Z. OESTERLEN: *Z. Metallkd.*, 1938, **30**, 386.
99. C. E. RANSLEY and D. E. J. TALBOT: *Z. Metallkd.*, 1955, **46**, 378.
100. D. STEPHENSON: PhD thesis, Brunel University, UK, 1978.
101. H. SHAHANI: PhD thesis, Royal Institute of Technology, Stockholm, Sweden, 1984.
102. J. KOCUR, K. TOMASEK, and L. RABATIN: *Hutn. Listy*, 1989, **44**, 269.
103. D. E. J. TALBOT and P. N. ANYALEBECHI: *Mater. Sci. Technol.*, 1988, **4**, (1), 1.
104. H. LIU, L. ZHANG, and B. BOUCHARD: in 'Recent developments in light metals', (ed. M. Gilbert et al.), 257; 1994, Montreal, Canadian Institute of Metallurgists.
105. S. A. GEDEON and T. W. EAGAR: *Weld. J.*, 1990, **69**, 264s.
106. P. N. ANYALEBECHI: *Scr. Metall. Mater.*, 1995, **33**, (8), 1209.
107. Q. T. FANG, P. N. ANYALEBECHI, and D. A. GRANGER: Proc. TMS Annual Meeting on 'Light metals', 1988, 477-486.
108. P. M. THOMAS and J. E. GRUZLESKI: *Metall. Trans. B*, 1978, **9B**, 139.
109. J. H. VACCARI: *Am. Mach.*, Feb. 1991, 139.
110. G. E. METCALFE: *J. Inst. Met.*, 1945, **71**, 618.
111. M. PASTOR: MS thesis, The Pennsylvania State University, PA, USA, 1998.
112. LORD RAYLEIGH: *Philos. Mag.*, 1917, **34**, (6), 94.
113. G. K. BATCHELOR: 'An introduction to fluid dynamics', 490; 1967, Cambridge, Cambridge University Press.
114. J. KROOS, U. GRATZKE, and G. SIMON: *J. Phys. D: Appl. Phys.*, 1993, **26**, 474.
115. R. DUCHARME, P. KAPADIA, and J. DOWDEN: Proc. ICALEO '93: 'Laser materials processing', (ed. P. Denney et al.), 177; 1993, Orlando, Florida, Laser Institute of America.
116. R. DUCHARME et al.: Proc. ICALEO '92: 'Laser materials processing', (ed. D. Farson et al.), 177; 1992, Orlando, FL, Laser Institute of America.
117. A. MATSUNAWA, S. KATAYAMA, H. IKEDA, and K. NISHIZAWA: Proc. ICALEO '92: 'Laser materials processing', (ed. D. Farson et al.), 547; 1992, Orlando, FL, Laser Institute of America.
118. D. A. SCHAUER and W. H. GIEDT: *Weld. J.*, 1978, **57**, (7), 189s.
119. S. KATAYAMA and C. D. LUNDIN: *J. Light Met. Weld. Constr.*, 1991, **29**, (9), 1-13.
120. M. KUTSUNA: Proc. 27th ISATA: 'Automotive technology and automation', Aachen, Germany, October-November 1994, 427.
121. J. O. MILEWSKI, G. K. LEWIS, and J. E. WITTIG: *Weld. J.*, 1993, **72**, 341s-346s.
122. J. C. LIPPOLD: Proc. Taiwan Int. Welding Conf. on 'Technology advancements and new industrial applications in welding', September 1998, 35-46.
123. J. C. BORLAND and R. N. YOUNGER: *Br. Weld. J.*, 1960, **7**, 22-59.
124. J. C. BORLAND: *Br. Weld. J.*, 1961, **8**, (11), 526-540.
125. D. VAN DER TORRE and N. M. J. ROMIJN: Doc. IX-526-67, IIW, Paris, France, 1967.
126. J. A. WILLIAMS and A. R. E. SINGER: *J. Austr. Inst. Met.*, 1966, **11**, (1), 2-9.
127. J. C. BORLAND: *Br. Weld. J.*, 1960, **7**, 508-512.
128. F. MATSUDA, H. NAKAGAWA, and K. SONODA: *Trans. JWRI*, 1982, **11**, (2), 67-77.
129. J. H. DUDAS and F. R. COLLINS: *Weld. J.*, 1966, **45**, 241s-249s.
130. R. A. PATTERSON and J. O. MILEWSKI: *Weld. J.*, 1985, **64**, 227s-231s.
131. G. M. ECAR and H. D. BRODY: in 'Trends in welding research in the United States', (ed. S. A. David), 399-417; 1982, Metals Park, OH, ASM.
132. U. I. BIRMAN and A. V. PETROV: *SVAR Proiz.*, 1971, (6), 14-17.
133. L. GUITERREZ, G. NEYE, and E. ZSCHECH: *Weld. J.*, 1996, **75**, (4), 115s-121s.
134. I. STOL: *Weld. J.*, 1994, **73**, 57-65.
135. T. WATANABE, Y. YOSHIDA, and T. ARAI: Proc. Int. Conf. on 'Laser advanced materials processing', Nagaoka, Japan, 1992, 505-510.
136. H. YUNJIA, R. H. FROST, D. L. OLSON, and G. R. EDWARDS: *Weld. J.*, 1989, **68**, 280s-289s.
137. F. MATSUDA, H. NAKAGAWA, K. NAKATA, and R. AYANI: *Trans. JWRI*, 1978, **7**, 181.
138. S. VENKATARAMAN, J. H. DEVLETIAN, W. E. WOOD, and D. G. ATTERIDGE: in 'Grain refinement in castings and welds', (ed. G. J. Abbaschian and S. A. David), 275; 1983, Warrendale, PA, TMS.
139. M. E. WELLS and W. Z. LUKENS: *Weld. J.*, 1986, **65**, 314s.
140. F. MATSUDA: in 'Recent trends in welding science and technology', (ed. S. A. David and J. M. Vitek), 127-136; 1989, Materials Park, OH, ASM International.
141. S. KOU: in 'Recent trends in welding science and technology', (ed. S. A. David and J. M. Vitek), 137-146; 1989, Materials Park, OH, ASM International.
142. K. H. LEONG, K. R. SABO, P. G. SANDERS, and W. J. SPAWR: in 'Lasers as tools for manufacturing II', (ed. L. R. Miglione and R. D. Schaeffer), SPIE Proc. 2993, 37-44; 1997, Bellingham, WA, International Society for Optical Engineering.
143. E. A. BRANDES: 'Smithells metals reference book', 6th edn; 1983, London, Butterworth (in association with Fulmer Research Institute).
144. Y. S. TOULOUKIAN: 'Thermophysical properties of high temperature solid materials', Vol. 1; 1967, New York, Macmillan.